Theoretical *z*-pinch scaling relations for thermonuclear-fusion experiments

W. A. Stygar, M. E. Cuneo, R. A. Vesey, H. C. Ives, M. G. Mazarakis, G. A. Chandler, D. L. Fehl, R. J. Leeper, M. K. Matzen, D. H. McDaniel, J. S. McGurn, J. L. McKenney, D. J. Muron, C. L. Olson, J. L. Porter, J. J. Ramirez, J. F. Seamen, C. S. Speas, R. B. Spielman, K. W. Struve, J. A. Torres, and E. M. Waisman
Sandia National Laboratories, Albuquerque, New Mexico 87185-1196, USA

T. C. Wagoner and T. L. Gilliland
Ktech Corporation, Albuquerque, New Mexico 87123-3336, USA
(Received 21 June 2004; revised manuscript received 7 March 2005; published 8 August 2005)

We have developed wire-array *z*-pinch scaling relations for plasma-physics and inertial-confinement-fusion (ICF) experiments. The relations can be applied to the design of *z*-pinch accelerators for high-fusion-yield (~0.4 GJ/shot) and inertial-fusion-energy (~3 GJ/shot) research. We find that $(\delta_a/\delta_{\mathrm{RT}}) \propto (m/\ell)^{1/4}(R\Gamma)^{-1/2}$, where δ_a is the imploding-sheath thickness of a wire-ablation-dominated pinch, δ_{RT} is the sheath thickness of a Rayleigh-Taylor-dominated pinch, m is the total wire-array mass, ℓ is the axial length of the array, R is the initial array radius, and Γ is a dimensionless functional of the shape of the current pulse that drives the pinch implosion. When the product $R\Gamma$ is held constant the sheath thickness is, at sufficiently large values of m/ℓ, determined primarily by wire ablation. For an ablation-dominated pinch, we estimate that the peak radiated x-ray power $P_r \propto (I/\tau_i)^{3/2} R\ell\Phi\Gamma$, where I is the peak pinch current, τ_i is the pinch implosion time, and Φ is a dimensionless functional of the current-pulse shape. This scaling relation is consistent with experiment when 13 MA $\leqslant I \leqslant$ 20 MA, 93 ns $\leqslant \tau_i \leqslant$ 169 ns, 10 mm $\leqslant R \leqslant$ 20 mm, 10 mm $\leqslant \ell \leqslant$ 20 mm, and 2.0 mg/cm $\leqslant m/\ell \leqslant$ 7.3 mg/cm. Assuming an ablation-dominated pinch and that $R\ell\Phi\Gamma$ is held constant, we find that the x-ray-power efficiency $\eta_x \equiv P_r/P_a$ of a coupled pinch-accelerator system is proportional to $(\tau_i P_r^{7/9})^{-1}$, where P_a is the peak accelerator power. The pinch current and accelerator power required to achieve a given value of P_r are proportional to τ_i, and the requisite accelerator energy E_a is proportional to τ_i^2. These results suggest that the performance of an ablation-dominated pinch, and the efficiency of a coupled pinch-accelerator system, can be improved substantially by decreasing the implosion time τ_i. For an accelerator coupled to a double-pinch-driven hohlraum that drives the implosion of an ICF fuel capsule, we find that the accelerator power and energy required to achieve high-yield fusion scale as $\tau_i^{0.36}$ and $\tau_i^{1.36}$, respectively. Thus the accelerator requirements decrease as the implosion time is decreased. However, the x-ray-power and thermonuclear-yield efficiencies of such a coupled system increase with τ_i. We also find that increasing the anode-cathode gap of the pinch from 2 to 4 mm increases the requisite values of P_a and E_a by as much as a factor of 2.

DOI: 10.1103/PhysRevE.72.026404 PACS number(s): 52.58.Lq, 52.59.Qy, 52.25.Os, 84.70.+p

I. INTRODUCTION

High-yield thermonuclear fusion can in principle be achieved using x rays radiated by a petawatt-class *z*-pinch driver. In one approach to *z*-pinch-driven fusion, radiation from two colinear pinches heats a centrally located hohlraum that contains an inertial-confinement-fusion (ICF) fuel capsule [1–12]. The geometry of such a system is illustrated in Fig. 1.

According to the original computational study of a double-pinch-driven hohlraum, this system requires that the total x-ray power radiated by the two pinches reach 2400 TW in a 7-ns pulse to achieve a one-dimensional (1D) thermonuclear yield of 0.40 GJ [1]. (This assumes that the coaxial anode-cathode gap of the pinch, as defined in Fig. 1, is 2 mm [1].) Higher-resolution simulations with an improved capsule design find that 1800 TW in a 10-ns pulse would be required to achieve a 0.53-GJ yield [11,12]. The ultimate application of *z*-pinch-driven fusion would be inertial fusion energy—i.e., commercial power production, which would require yields on the order of 3 GJ [13,14]. Petawatt x-ray sources are also of interest to radiation-hydrodynamics, radiation-transport, astrophysics, and other plasma-physics experiments [15–17].

Tungsten-wire-array pinches relevant to *z*-pinch-driven ICF research presently radiate as much as 130 TW in a 12.5-ns pulse for experiments conducted at currents as high as 19 MA on the Z pulsed-power accelerator [3–10,16,18–33]. (The Z accelerator is the highest-current 100-ns pulse generator developed to date [34–42].) The pinches have a small initial radius (10 mm) and axial length (10 mm) to minimize the size of the hohlraum and maximize the radiation-drive temperature. To make efficient use of the Z-accelerator power pulse, pinch implosion times are on the order of the accelerator's 100-ns current-pulse width.

Higher-current machines are being proposed to increase the peak radiated x-ray power [43–45]. As presently envisioned, these would have 100–120 ns implosion times. However, it is necessary to consider a *z*-pinch accelerator, a double-pinch-driven hohlraum, and an ICF fuel capsule as a coupled system, and it is not clear that 100–120-ns implosions would optimize the performance of such a system for ICF applications.

To determine the range of optimum implosion times would require an understanding of how the peak radiated

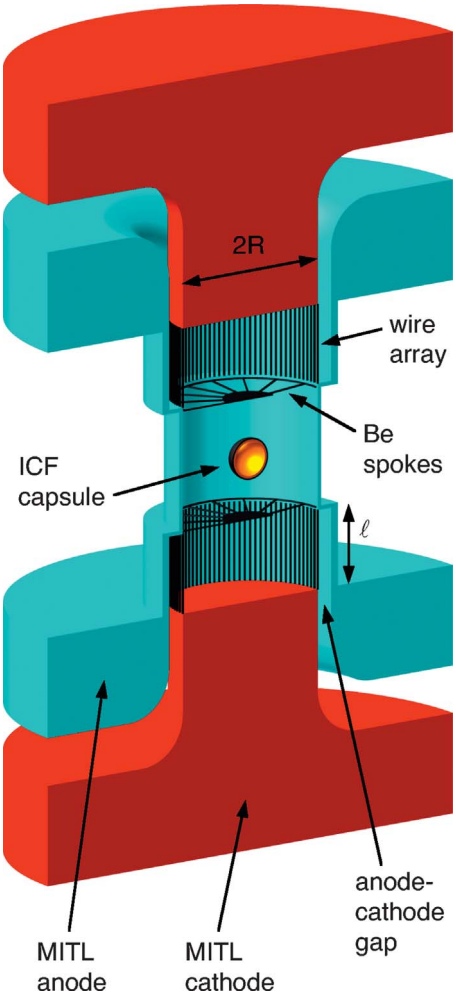

FIG. 1. (Color) Cross-sectional view of an idealized double-pinch-driven hohlraum system. Two colinear wire-array pinches drive the centrally located hohlraum, which contains an ICF fuel capsule. The quantities R and ℓ are the initial array radius and the array length, respectively. Two magnetically insulated vacuum transmission lines (MITL's) deliver current to the two pinches, which are electrically in parallel.

x-ray power P_r and x-ray-power pulse width τ_w vary with the peak pinch current I, pinch implosion time τ_i, initial wire-array radius R, and other pinch parameters. A complete theoretical understanding will likely require a systematic set of *predictive* three-dimensional wire-array simulations [24,25,27–33,46–56].

Until such simulations are available, it might be useful to consider the scaling relations developed in Sec. II A. These estimate P_r, τ_w, the total radiated x-ray energy E_r, pinch-energy thermalization time τ_{th}, radial thickness of the imploding pinch plasma δ_a, and pinch radius at stagnation a for a wire-array z pinch as functions of I, τ_i, R, and other parameters.

The relations developed in Sec. II A assume an *idealized* ablation-dominated pinch—i.e., a pinch for which the imploding sheath thickness is determined primarily by wire-ablation effects. Section II A generalizes and extends the ideas outlined in Ref. [29], and is motivated by arguments developed by Yadlowski *et al.* [46], Chittenden *et al.* [47,48,51,55], Lebedev *et al.* [49,52,56], Aleksandrov *et al.* [50,54], Cuneo *et al.* [24,32], Mazarakis *et al.* [25,27,28,33], Reisman *et al.* [53], Waisman *et al.* [30], and Sinars *et al.* [31].

We caution that given the complex three-dimensional time-dependent nature of the wire-ablation, implosion, and stagnation processes, the scaling relations developed in Sec. II A can be accurate to at most first order ($\sim 10\% - 20\%$) and only over a limited parameter regime. The relations are being presented as a first approximation and are intended to motivate considerably more accurate and more general calculations, and additional experiments.

Section II A assumes that the characteristic time required to ablate the wires in an array is a significant fraction of the implosion time, and as a result, the sheath thickness of the imploding wire-array plasma is determined primarily by wire ablation. When the ablation time is much less than the implosion time, the sheath thickness is determined by the Rayleigh-Taylor (RT) instability and other sheath-broadening mechanisms. In Sec. II B, we present scaling relations for an *idealized* RT-dominated pinch [57] and contrast these to the relations obtained in Sec. II A. In Sec. II C we compare the P_r scaling relations developed in Secs. II A and II B (for ablation- and RT-dominated pinches, respectively) to experiments conducted with tungsten wire arrays that have parameters of interest to ICF research.

A wire-array z-pinch implosion with a peak current in excess of a few MA is typically driven by a multimodule pulsed-power accelerator. Each module of such an accelerator delivers an electromagnetic power pulse to a radial-transmission-line system. The radial system is usually located at the center of the accelerator and includes the z-pinch load. The output electromagnetic-power pulses produced by all of the accelerator's modules are added at the interface between the modules and the radial-transmission-line system; the radial system delivers a significant fraction of this combined power to the pinch.

In Sec. III we estimate the peak accelerator power at the radial-system interface P_a that is required to achieve a peak pinch current I and implosion time τ_i. Using this result and the estimate for P_r given in Sec. II A, we develop in Sec. III an expression for the *x-ray-power efficiency* of a *coupled pinch-accelerator system*. We also develop scaling relations for the values of P_a, the accelerator energy delivered to the radial system E_a, the peak interface voltage V, and the radial-system inductance L that would be required to achieve a given value of P_r.

To realize high-yield ICF will require not only that P_r but also that the x-ray-power pulse width τ_w meet certain requirements. To determine how these might be met, we consider in Sec. IV an accelerator that drives two z pinches in a double-pinch-driven hohlraum, and assume that the hohlraum radiation in turn drives the implosion of an ICF fuel capsule [1,11,12]. Using the results of Secs. II and III, we develop in Sec. IV an expression for the *thermonuclear-yield efficiency* of such a *coupled capsule-hohlraum-accelerator system*. We also develop scaling relations for the values of P_r, I, τ_i, P_a, E_a, V, and L that would be required to access the conditions necessary for high-yield fusion.

In Sec. V we develop quantitative estimates of the pinch and accelerator parameters that would be required to achieve

high yield, assuming that when $R=\ell=10$ mm, the anode-cathode gap of the pinch is 2 mm [1]. Recent experiments suggest that gaps larger than 2 mm may be necessary at the pinch currents required to achieve high yield [29]. Hence in Sec. V we also estimate the requisite pinch and accelerator parameters assuming a 4-mm gap.

The results presented in Secs. II–V, and suggestions for future work, are discussed in Sec. VI.

II. THEORETICAL z-PINCH SCALING RELATIONS

A. Idealized ablation-dominated pinch

In this section we consider a single ablation-dominated wire-array z pinch—i.e., a pinch for which the effective radial thickness of the imploding wire-array plasma is determined primarily by wire-ablation effects. We assume here that the RT instability and other sheath-broadening mechanisms can be neglected.

Preliminary scaling relations for an ablation-dominated pinch are developed in Sec. III C 2 of Ref. [29]. These assume that the wire material, initial wire-mass density, initial wire-array radius R, wire-array length ℓ, effective final pinch radius a, and normalized pinch current $F=F(r/R)$ are held constant [29]. The quantities R and ℓ are defined in Fig. 1. We define $F(r/R)$ as $I(r/R)/I$, where $I(r/R)$ is the pinch current as a function of r/R, r is an effective time-dependent radius of the imploding wire-array plasma, and I is the peak pinch current. The scaling relations given in [29] also assume that the number of wires n is near the value that optimizes the peak radiated x-ray power.

In the discussion below, we generalize the preliminary study of Ref. [29] to allow for variations in R, ℓ, and a; in addition, the following discussion differs somewhat from that presented previously.

We begin by assuming that the peak x-ray power radiated by an ablation-dominated pinch is proportional to E_r/τ_{th}:

$$P_r \propto \frac{E_r}{\tau_{th}}, \tag{1}$$

where E_r is the total x-ray energy radiated by the pinch, and τ_{th} is a characteristic time over which the energy made available to the pinch is thermalized.

Two-dimensional magnetohydrodynamic (MHD) imploding-pinch simulations performed in the r-z plane suggest that E_r is, to a good approximation, equal to the total work performed by the $\mathbf{j}\times\mathbf{B}$ force on the pinch plasma [58]. The $\mathbf{j}\times\mathbf{B}$ work flows first into kinetic energy and subsequently into the internal energy of the pinch. As indicated in Ref. [58], this occurs while energy leaves the pinch through radiation. Although the pinch kinetic energy obtained from 0D and 1D calculations is substantially less than the measured radiated x-ray energy, such a discrepancy does not exist for the more accurate 2D calculations [58]. For the cases considered in Ref. [58], the total radiated x-ray energy is approximately equal to the total $\mathbf{j}\times\mathbf{B}$ work performed on the pinch.

However, the simulations described in [58] apply to an RT-dominated pinch and do not include effects due to wire ablation, a three-dimensional process [24,25,27–33,46–56]. Until 3D simulations are available with adequate spatial resolution, temporal resolution, numerical energy conservation, etc., we make the simplifying assumption that E_r is *proportional* to a *characteristic* value of the kinetic energy delivered to the pinch E_k, which we define as follows:

$$E_r \propto E_k \equiv \frac{1}{2} m v_p^2, \tag{2}$$

where m is the total wire-array mass and v_p is an *effective* peak sheath velocity (the effective value of the highest velocity attained by the pinch mass). We also assume that v_p is sufficient to enable highly efficient thermalization of the energy delivered to the pinch.

We approximate E_k as the work performed by an idealized azimuthal magnetic field on a thin imploding annular plasma:

$$\frac{1}{2} m v_p^2 = \frac{-\mu_0 \ell I^2}{4\pi} \int_1^{a/R} \frac{F^2(r/R)\, d(r/R)}{(r/R)} \equiv \frac{\mu_0 \ell I^2}{4\pi} \Phi, \tag{3}$$

where μ_0 is the free-space magnetic permeability and $\Phi = \Phi[F(r/R),(a/R)]$. The radius a is an effective final pinch radius at which the pinch stagnates and the energy made available to the pinch is thermalized. Equations are in SI units throughout.

The dimensionless quantity Φ is a functional of $F(r/R)$ and the pinch convergence ratio a/R. When $F(r/R)$ is a physically reasonable function and $(a/R) \ll 1$, Φ is a weak function of a/R. For example, when $F(r/R)=1$, $\Phi = \ln(R/a)$.

When $(a/R) \ll 1$ and r/R is expressed as an explicit function of the dimensionless variable t/τ_i (where τ_i is the pinch implosion time, defined later in this section), then $F(r/R)$ becomes $f(t/\tau_i)$, where $f(t/\tau_i) \equiv I(t/\tau_i)/I$ and $I(t/\tau_i)$ is the pinch current as a function of t/τ_i.

The functions $F(r/R)$ and $f(t/\tau_i)$ are the normalized pinch currents expressed as functions of the dimensionless quantities r/R and t/τ_i, respectively. We define $G(r)$ and $g(t)$ as the normalized currents expressed as functions of r and t. In this article, we consider pinches with implosions for which the functions $G(r)$ are *similar* [59]—i.e., differ only by a similarity transformation. For such pinches the *shapes* of the normalized currents $G(r)$ are held constant, differing only by the scale factor R. Hence, for similar pinches, the function $F(r/R)$ is held constant. It is straightforward to show that when $a/R \ll 1$, holding $F(r/R)$ constant is equivalent to holding $f(t/\tau_i)$ constant. Under these conditions, the shapes of the functions $g(t)$ also remain constant and differ only by a similarity transformation—i.e., by the scale factor τ_i. In addition, the implosion-velocity profiles $v(r/R)$ differ only by their amplitudes, which scale as R/τ_i; this is also true for the implosion-velocity time histories $v(t/\tau_i)$.

For pinches with similar implosions, we assume τ_{th} of Eq. (1) is determined primarily by two variables: the characteristic sheath velocity R/τ_i and a characteristic radial thickness of the imploding wire-array plasma, δ_a. [We assume δ_a is the sheath thickness averaged azimuthally (over ϑ) and over the

axial length of the pinch ℓ. We also assume ℓ is much longer than the characteristic length of axial variations in the sheath thickness.] Hence dimensional analysis gives

$$\frac{\tau_{th}}{\tau_i} \propto \frac{\delta_a}{R}. \tag{4}$$

For similar pinches τ_{th}/τ_i can only be a function of δ_a/R, which is consistent with Eq. (4).

For ablation-dominated pinches, we assume δ_a is determined primarily by two variables: the characteristic sheath velocity R/τ_i and a characteristic time required to ablate the wires τ_a. (We define τ_a to be the ablation time averaged over ϑ and ℓ, and that ℓ is much longer than the characteristic length of axial variations in the ablation.) Hence

$$\frac{\delta_a}{R} \propto \frac{\tau_a}{\tau_i}. \tag{5}$$

For similar pinches δ_a/R can only be a function of τ_a/τ_i, which is consistent with Eq. (5).

Equation (5) agrees with qualitative expectations. When the ablation time is much less than the implosion time ($\tau_a/\tau_i \ll 1$) and the number of wires is sufficiently large to provide azimuthal symmetry, we expect that a thin annular shell forms early in time. Assuming that the shell is axisymmetric, the thickness of the shell (in the absence of RT) remains thin as it implodes, as has been demonstrated with 2D (r-z) MHD simulations. As the ratio τ_a/τ_i is increased, we expect that the mass assembly on axis becomes more diffuse and less well defined due to trailing mass, parasitic currents, axial and azimuthal variations in the ablation rate, etc. [24,25,27–33,46–56]. These arguments suggest that δ_a is an increasing function of τ_a, which is consistent with Eq. (5).

To estimate the ablation time τ_a, we consider first the ablation of a single wire, not in an array. Analytic calculations by Bobrova, Razinkova, and Sasorov [60] predict that the ablation of a single frozen-deuterium filament is described by the following relations:

$$\frac{1}{\ell}\left(\frac{dm_s(t)}{dt}\right) \propto \left(\frac{dI_s(t)}{dt}\right)^{\kappa/\gamma} t^{(1-\gamma)/\gamma}, \tag{6}$$

$$\tau_a \propto \frac{(m_s/\ell)^{\gamma}}{[dI_s(t)/dt]^{\kappa}}, \tag{7}$$

where $m_s(t)$ is the time-dependent mass of a single filament, $I_s(t)$ is the current flowing in the filament, γ and κ are constants, and m_s is the initial filament mass. Equations (6) and (7) assume that (i) the filament is not in an array, (ii) the filament material and initial filament mass density are held constant, and (iii) $I_s(0)=0$ for $t<0$ and $I_s(t) \propto t$ for $t \geqslant 0$. Under these three conditions, τ_a can only be a function of the two quantities m_s/ℓ and $dI_s(t)/dt$, which is consistent with Eq. (7).

For a filament or wire that is part of an array, τ_a is also a function of the array's magnetic-field topology—specifically, the ratio of the array's global magnetic field to the field in the vicinity of an individual wire [47]. For the discussion in this article, we consider only arrays for which the range of ratios is sufficiently small that *changes* in τ_a between configurations are dominated by changes in m_s/ℓ and $dI_s(t)/dt$, and that effects due to changes in the topologies between arrays of interest can be neglected.

According to numerical calculations performed by Lindemuth, McCall, and Nebel [61], the time required to ablate a single frozen deuterium wire scales as $\tau_a \propto (m_s/\ell)^{1/2}$, when the wire material, initial wire-mass density, and the value of $dI_s(t)/dt$ are held constant. Since the total mass of a wire array $m=nm_s$ where n is the number of wires, and $I(t)=nI_s(t)$ where $I(t)$ is the total wire-array current as a function of time, we can write Eq. (7) as

$$\tau_a \propto \frac{(m/n\ell)^{1/2}}{[dI(t)/ndt]^{\kappa}}. \tag{8}$$

Using Eqs. (4), (5), and (8), we approximate the thermalization time τ_{th} as

$$\tau_{th} \propto \frac{(m/n\ell)^{1/2}}{[dI(t)/ndt]^{\kappa}}. \tag{9}$$

Coverdale and colleagues [62] have demonstrated that for aluminum-wire arrays, there exists an optimum value of n that maximizes P_r—i.e., that P_r does not continue to increase indefinitely as n is increased. Mazarakis and co-workers [25,27,28,33] have shown that an optimum n also exists for the $R=10$ mm, $\ell=10$ mm tungsten-wire array presently being developed as the driver for the double-pinch-driven hohlraum. A polynomial fit [25,27,28,33] to the data suggests that P_r has a broad maximum at $n \sim 355$ and that P_r varies from 130 to 133 TW for $300 \leqslant n \leqslant 400$. The fit suggests that the peak x-ray power drops to 112 TW at $n=220$ and also at $n=480$.

When n is much less than the optimum value, it appears that the azimuthal asymmetry introduced by the discrete wires of an array compromises the radial implosion [63,64]. An increase in n significantly above the optimum may enable correlations of density perturbations in adjacent wires, which would enhance growth of the RT instability [25,27,28,33,56].

For this discussion, we consider conditions under which the optimum number of wires occurs in the ablation-dominated regime. As indicated by Eq. (31) in Sec. II B, this is likely to be the regime of most interest to double-pinch-driven ICF research. The double-pinch system requires massive small-initial-radius arrays; for such arrays presently in use at 17–19 MA, it appears that wire ablation dominates the implosion dynamics [24,29,31,32]. According to Eq. (31), when m/ℓ is increased for experiments conducted at higher currents on future accelerators, the effects of ablation will become even more significant.

Since P_r is proportional to E_r/τ_{th} [Eq. (1)], the expression for τ_{th} [Eq. (9)] is approximately independent of n for arrays that have a near-optimum number of wires. Hence for such arrays $\kappa \sim 1/2$, and we can write Eqs. (6), (8), and (9) as follows:

$$\frac{1}{\ell}\left(\frac{dm(t)}{dt}\right) \propto \left(\frac{dI(t)}{dt}\right) t, \tag{10}$$

$$\tau_{th} \propto \tau_a \propto \left(\frac{m/\ell}{dI(t)/dt}\right)^{1/2} \propto \left(\frac{m\tau_i}{\ell I}\right)^{1/2}, \tag{11}$$

where $m(t) \equiv n m_s(t)$. Although Eq. (10) is motivated in part by *calculations* assuming *cryogenic deuterium*, it is also consistent (to within experimental uncertainties) with direct x-ray radiographic *measurements* of the ablation of *tungsten* wires with initial diameters that range between 7.5 and 40 μm, driven by currents with nominal values of $dI(t)/dt$ per wire that range between $\sim$0.25 and $\sim$2 kA/ns [65].

Equation (11) assumes that the rise time of the current pulse is proportional to the pinch implosion time τ_i, which is valid for similar implosions. We define τ_i as follows:

$$\tau_i \equiv \int_R^a \frac{dr}{v(r)}, \tag{12}$$

where $v(r)$ is a characteristic velocity of the imploding pinch plasma as a function of r. For a thin imploding annular plasma, we estimate that

$$\tau_i = -\left(\frac{2\pi m}{\mu_0 \ell}\right)^{1/2} \frac{R}{I} \int_1^{a/R} \frac{d(\rho/R)}{\left[-\int_1^{\rho/R} \frac{F^2(r/R)d(r/R)}{(r/R)}\right]^{1/2}} \equiv \left(\frac{2\pi m}{\mu_0 \ell}\right)^{1/2} \frac{R}{I} \Gamma, \tag{13}$$

where $\Gamma = \Gamma[F(r/R), (a/R)]$.

The dimensionless quantity Γ is a functional of $F(r/R)$ and the pinch convergence ratio a/R. When $F(r/R)$ is a physically reasonable function and $(a/R) \ll 1$, Γ is a much weaker function of a/R than is Φ. For example, when $F(r/R)=1$ and $(a/R) \to 0$, Γ approaches a constant value, whereas $\Phi \propto \ln(R/a) \to \infty$.

Combining Eqs. (1)–(5), (11), and (13), we obtain the following approximate expressions for an ablation-dominated wire-array pinch:

$$P_r \propto \left(\frac{\ell}{m}\right)^{3/4} \frac{I^3 \ell \Phi}{(R\Gamma)^{1/2}} \propto \left(\frac{I}{\tau_i}\right)^{3/2} R\ell\Phi\Gamma, \tag{14}$$

$$E_r \propto I^2 \ell \Phi, \tag{15}$$

$$\tau_{th} \propto \tau_a \propto \left(\frac{m}{\ell}\right)^{3/4} \frac{(R\Gamma)^{1/2}}{I} \propto \frac{I^{1/2}\tau_i^{3/2}}{R\Gamma}, \tag{16}$$

$$\delta_a \propto \left(\frac{m}{\ell}\right)^{1/4} \left(\frac{R}{\Gamma}\right)^{1/2} \propto \frac{(I\tau_i)^{1/2}}{\Gamma}, \tag{17}$$

$$\tau_i \propto \left(\frac{m}{\ell}\right)^{1/2} \frac{R\Gamma}{I}. \tag{18}$$

As discussed above, Eqs. (14)–(18) assume that (i) the wire material and initial wire-mass density are held constant, (ii) v_p is sufficiently high to achieve efficient thermalization of the energy delivered to the pinch, (iii) the characteristic radial thickness of the imploding pinch plasma is determined primarily by wire-ablation effects, (iv) the quantity $F(r/R)$ [or equivalently $f(t/\tau_i)$] is held constant, so that the pinch implosions under consideration are similar, and (v) the number of wires n is near the value that optimizes P_r. When the quantities R, ℓ, Φ, and Γ are held constant, Eqs. (14), (16), and (17) are identical to Eqs. (24)–(26) of Ref. [29].

If we define the effective width of the x-ray-power pulse τ_w as [29,66]

$$\tau_w \equiv \frac{E_r}{P_r}, \tag{19}$$

we obtain from Eqs. (1) and (19) that

$$\tau_w \propto \tau_{th}, \tag{20}$$

where τ_{th} is given by Eq. (16). For the pinch model described by Eqs. (14)–(18), the definition of pulse width given by Eq. (19) (proposed by Desjarlais [66]) is more natural and meaningful than the usual full width at half maximum. Adopting the definition given by Eq. (19) guarantees that $E_r = P_r \tau_w$; in addition, Eq. (19) accounts for the effective broadening of the x-ray-power pulse when a significant fraction of the radiated energy is in the pulse's tail.

For similar implosions $F(r/R)$ is held constant, and as indicated by Eqs. (3) and (13), the quantities Φ and Γ are functions only of the ratio a/R. (As noted earlier, Φ and Γ are *weak* functions of a/R when $a/R \ll 1$.) The ratio a/R scales as

$$\frac{a}{R} \propto \frac{\delta_a}{R} \tag{21}$$

for similar systems. Hence Eqs. (3), (13), and (21) indicate that Φ and Γ are functions only of δ_a/R, and decrease as δ_a/R is increased.

B. Idealized RT-dominated pinch

Equations (14)–(18), (20), and (21) are applicable to an idealized pinch with a sheath thickness determined primarily by wire-ablation effects. In the discussion below, we develop relations applicable to a pinch with a sheath thickness determined by the Rayleigh-Taylor instability.

We consider an axisymmetric pinch for which the *initial* sheath thickness $\delta_i \ll R$. We assume that there exist perturbations in the initial sheath radius that extend over the entire length of the pinch and that these seed RT growth. (Such perturbations are usually realized in 2D MHD simulations by including mass-density variations in a sheath with inner and outer surfaces that are smooth at $t=0$ [67–69].) We assume that the perturbations have the broadest possible wave-number spectrum, and that the initial amplitude of the perturbations A_i is independent of the perturbation wavelength.

We expect that the characteristic thickness of an RT-dominated sheath just before stagnation δ_{RT} is proportional to the final amplitude A_f of the perturbations that experience the greatest growth:

$$\delta_{\mathrm{RT}} \propto A_f \propto \xi A_i, \tag{22}$$

where ξ is the factor by which the amplitude has increased from its initial value. We define δ_{RT} to be the sheath thickness averaged azimuthally (over ϑ) and over the axial length of the pinch ℓ.

We make the simplifying assumption that for pinches of interest, the wavelengths that ultimately contribute the most to the broadening of a sheath are sufficiently large that the effects of resistivity, viscosity, compressibility, initial density gradients, etc., can be neglected [57,67–69]. Under these conditions, we expect that the growth factor ξ is a functional of only the following independent quantities: δ_i, A_i, R, τ_i, ℓ, and $F(r/R)$. We assume that, once defined, these quantities uniquely determine—to within chaotic fluctuations—the evolution of the large-wavelength modes.

Two-dimensional MHD simulations by Marder, Sanford, and Allshouse [70] demonstrate that the sheath thickness just before stagnation δ_{RT} is a weak function of δ_i when $\delta_i \ll R$. Since we limit our discussion to such pinches, we assume that the dependence of ξ on δ_i can be neglected. Since ξ is independent of ℓ when the wavelengths of the most damaging modes are much less than ℓ (which is usually the case), we neglect the dependence of ξ on ℓ. In addition, we consider only pinches with similar implosions—i.e., for which $F(r/R)$ is held constant.

Under these conditions, since ξ is dimensionless, it can only be a function of A_i/R. If we further restrict our discussion to pinches for which

$$A_i \propto R, \tag{23}$$

then ξ is constant and

$$\delta_{\mathrm{RT}} \propto R. \tag{24}$$

[It is straightforward to show that $A_i \propto R$ when the fractional perturbation level in the lineal mass density m/ℓ of a sheath (that is smooth and thin at $t=0$) is held constant.]

The arguments presented above were motivated by, and are consistent with, the results of Youngs [71,72] and Desjarlais and Marder [73].

Ryutov, Derzon, and Matzen [57] also assume $\delta_{\mathrm{RT}} \propto R$ for RT-dominated pinches that have similar implosions. We note that Refs. [57,71,72] consider systems for which the memory of the initial conditions is lost during nonlinear RT growth, so that the only relevant scale length is R. We assume instead that some dependence on A_i remains, but that $A_i \propto R$.

Equation (24) appears to be consistent with the results of 2D MHD pinch simulations presented in Fig. 8 of Ref. [74]. These find that when A_i/R is held approximately constant, the sheath thickness of an array with $R=20$ mm is, on average, a factor of ~ 1.6 greater than when $R=12.5$ mm.

When Eq. (24) is valid, then

$$a \propto R, \tag{25}$$

since there are no other relevant scale lengths.

Equations (24) and (25) assume that A_i/R is held constant; however, we caution that the initial perturbations are not well understood. In 2D (r-z) MHD pinch simulations conducted to date, the initial perturbation amplitude is simply adjusted until results match experiment [58,67–69]. Even when A_i/R is constant, Eqs. (24) and (25) can only be approximations, given the assumptions implicit in these equations. Nevertheless, it is interesting to consider an *idealized* RT-dominated pinch, which we define here as a pinch for which Eqs. (24) and (25) are applicable. This case likely provides an upper limit on the scaling of P_r with I as the peak current is increased on future accelerators.

Assuming Eqs. (24) and (25), we use arguments similar to those developed in Sec. II A to obtain the following expressions:

$$P_r \propto \left(\frac{\ell}{m}\right)^{1/2} \frac{I^3 \ell}{R} \propto \frac{I^2 \ell}{\tau_i}, \tag{26}$$

$$E_r \propto I^2 \ell, \tag{27}$$

$$\tau_{th} \propto \tau_w \propto \tau_i, \tag{28}$$

$$\delta_{\mathrm{RT}} \propto a \propto R, \tag{29}$$

$$\tau_i \propto \left(\frac{m}{\ell}\right)^{1/2} \frac{R}{I}. \tag{30}$$

Since $F(r/R)$ is constant for pinches with similar implosions and a/R is constant for similar RT-dominated pinches, the quantities Φ and Γ [defined by Eqs. (3) and (13), respectively] are also constant; hence Φ and Γ do not appear in Eqs. (26)–(30). We note that Eqs. (26)–(30) are valid only when Eqs. (24) and (25) are applicable, and v_p is sufficiently high to achieve efficient thermalization of the energy delivered to the pinch.

Equations (27) and (30) are similar to Eqs. (15) and (18), respectively. However, Eqs. (26), (28), and (29) differ substantially from Eqs. (14), (16), and (17). For example, as indicated by the last expressions of Eqs. (26) and (14), the ablation and RT models predict a significantly different scaling of P_r with the quantities I, τ_i, and R.

Although Eqs. (26) and (14) differ considerably, it is interesting to note that *both* models predict $P_r \propto I^3$ when m, ℓ, R, Φ, and Γ are held constant. To achieve this cubic current scaling would require that $\tau_i \propto I^{-1}$.

To determine when we might expect either ablation effects or RT to dominate the implosion dynamics of a pinch, we consider the ratio of δ_a to δ_{RT}:

$$\frac{\delta_a}{\delta_{\mathrm{RT}}} \propto \left(\frac{m}{\ell}\right)^{1/4} \frac{1}{(R\Gamma)^{1/2}}. \tag{31}$$

This ratio suggests that ablation dominates in massive small-initial-radius arrays, which are the arrays of most interest to z-pinch-driven ICF research. In addition, when the product $R\Gamma$ is held constant, Eq. (31) suggests that ablation dominates in *any* wire array configuration at a sufficiently large value of m/ℓ.

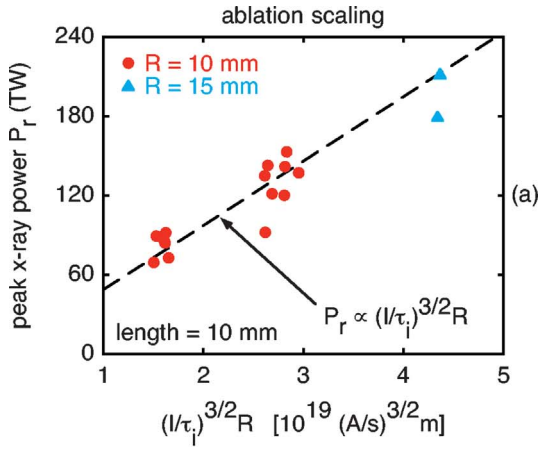

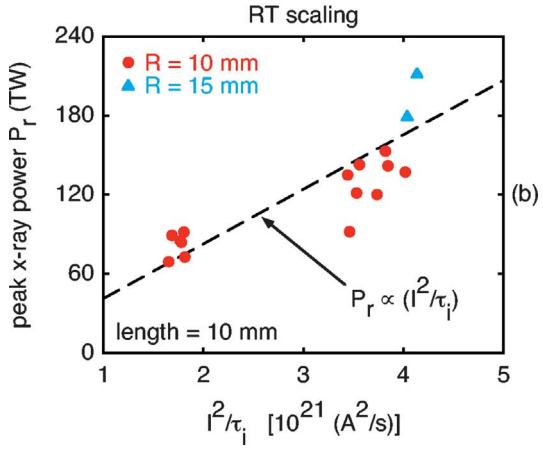

FIG. 2. (a) (Color) Measurements of the peak radiated x-ray power P_r as a function of $(I/\tau_i)^{3/2}R$, where I is the peak pinch current, τ_i is the implosion time, and R is the initial wire-array radius. The 16 measurements plotted in (a) are those listed in Table I with $\ell=10$ mm. For these measurements R is either 10 or 15 mm, I varies from 13 to 20 MA, τ_i from 93 to 100 ns, and m/ℓ from 2.6 to 5.9 mg/cm. These data are compared to the ablation-scaling relation given by Eq. (14), assuming that for these experiments, Φ and Γ are constant. It appears that the data are consistent with the ablation model to within the random shot-to-shot fluctuations in the measured values of P_r. (b) The peak x-ray-power P_r as a function of (I^2/τ_i) for the same set of data plotted in (a). In (b) the data are compared to the RT-scaling relation given by Eq. (26). It appears that the RT model is *not* consistent with the measurements.

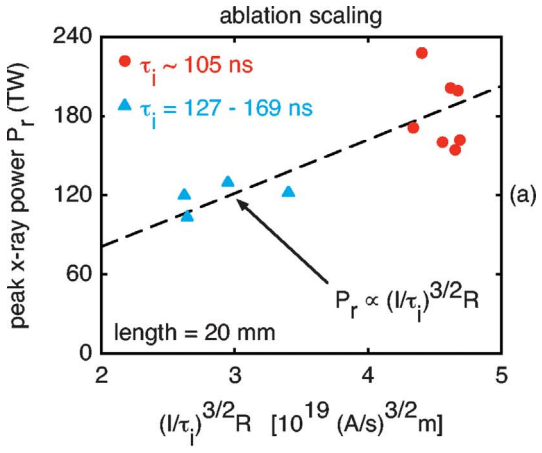

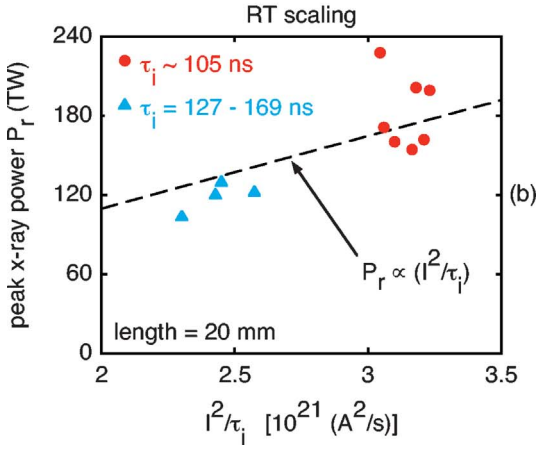

FIG. 3. (a) (Color) Measurements of the peak radiated x-ray power P_r as a function of $(I/\tau_i)^{3/2}R$, where I is the peak pinch current, τ_i is the implosion time, and R is the initial wire-array radius. The 11 measurements plotted in (a) are those listed in Table I with $\ell=20$ mm. For these measurements $R=20$ mm, I varies from 18 to 20 MA, τ_i from 103 to 169 ns, and m/ℓ from 2.0 to 7.3 mg/cm. These data are compared to the ablation-scaling relation given by Eq. (14), assuming that for these experiments, Φ and Γ are constant. It appears that the data are consistent with the ablation model to within the random shot-to-shot fluctuations in the measured values of P_r. (b) The peak x-ray-power P_r as a function of (I^2/τ_i) for the same set of data plotted in (a). In (b) the data are compared to the RT-scaling relation, Eq. (26). It appears that the RT model is slightly less consistent with the measurements.

C. Results

1. Comparison of the ablation and RT pinch models with experiment

In this section and Figs. 2 and 3, we compare the predictions of Secs. II A and II B with experimental results. The experiments [29,75–78] were conducted with tungsten-wire-array z pinches that have parameters of interest to ICF research; the results are summarized in Table I. The values listed in the table were estimated in a manner that is consistent with the process used to obtain the data presented in Ref. [29].

The 14 measurements listed in Table I with $\ell=10$ mm and $R=10$ mm are described in Ref. [29]; the 2 measurements with $\ell=10$ mm and $R=15$ mm were performed by Deeney *et al.* [76]. For these 16 $\ell=10$ mm measurements, I varies from 13 to 20 MA, τ_i from 93 to 100 ns, and m/ℓ from 2.6 to 5.9 mg/cm. Table I also lists measurements with $R=20$ mm [75,77,78]. The first of these (Z-shot 51) is described in Ref. [75]; shots 373–376 are described in Ref. [77]. For the 11 $R=20$ mm measurements listed in Table I, I varies from 18 to 20 MA, τ_i from 103 to 169 ns, and m/ℓ from 2.0 to 7.3 mg/cm.

In Fig. 2(a) we compare the 16 $\ell=10$ mm measurements

TABLE I. Summary of experimental results obtained with tungsten-wire-array z pinches [29,75–78]. The expressions Φ_{expt} and Γ_{expt}, defined by Eqs. (32) and (33), respectively, are dimensionless. For six of these shots, we do not list values of E_r, τ_w, and Φ_{expt}, since these quantities were affected by closure of the anode-cathode gap at the base of the pinch [29].

Axial pinch length ℓ	Z-shot number and reference	Initial wire-array radius R (mm)	Number of wires n	Total pinch mass m (mg)	Peak pinch current I (MA)	Pinch implosion time τ_i (ns)	Peak x-ray power P_r (TW)	Total x-energy E_r (MJ)	X-ray-power pulse width τ_w (ns)	Φ_{expt}	Γ_{expt}
	648 [29]	10	300	2.64	12.9	94	84				3.34
	820 [29]	10	300	2.72	13.1	95	92				3.35
	649 [29]	10	300	2.63	12.9	94	85	0.85	10.0	5.16	3.32
	647 [29]	10	300	2.62	12.6	96	69	0.81	11.6	5.08	3.34
	725 [29]	10	300	2.74	13.0	93	73	0.76	10.4	4.49	3.26
	819 [29]	10	300	2.74	12.7	96	89	0.86	9.7	5.36	3.29
	566 [29]	10	300	5.89	19.3	97	142				3.44
$\ell=10$ mm	597 [29]	10	300	5.86	19.5	95	137				3.42
	594 [29]	10	300	5.85	18.8	94	120				3.27
	683 [29]	10	300	5.85	18.1	96	135				3.21
	723 [29]	10	300	5.91	18.3	95	121	1.53	12.6	4.60	3.18
	724 [29]	10	300	5.87	19.1	95	153	1.76	11.5	4.83	3.36
	817 [29]	10	300	5.85	18.2	96	92	1.28	13.9	3.84	3.24
	818 [29]	10	300	5.87	18.6	97	143	1.70	11.9	4.90	3.35
	65 [76]	15	220	3.34	20.3	100	212	1.98	9.3	4.81	3.30
	66 [76]	15	220	3.34	19.9	98	180	2.17	12.1	5.48	3.18
	51 [75]	20	240	4.09	18.2	104	201	1.85	9.2	2.80	2.96
	161 [78]	20	240	4.05	18.2	103	162	1.29	8.0	1.95	2.95
	165 [78]	20	240	4.03	18.3	104	199	1.73	8.7	2.58	3.01
	168 [78]	20	240	4.06	18.0	106	228	1.91	8.4	2.95	3.00
	169 [78]	20	240	4.16	18.3	109	171	1.63	9.5	2.44	3.09
$\ell=20$ mm	234 [78]	20	240	3.97	17.9	103	160	1.33	8.3	2.07	2.94
	235 [78]	20	240	3.97	18.0	103	154	1.31	8.5	2.01	2.94
	373 [77]	20	480	8.57	18.9	146	131	1.65	12.7	2.31	2.98
	374 [77]	20	480	11.39	19.1	159	104	1.54	14.7	2.10	2.84
	375 [77]	20	480	14.66	20.3	169	121	1.86	15.4	2.26	2.83
	376 [77]	20	480	5.96	18.1	127	123	1.69	13.7	2.58	2.96

with Eq. (14); in Fig. 2(b), we compare the same measurements with Eq. (26). The theoretical curve plotted in Fig. 2(a) assumes that Φ and Γ are constant and that $P_r = c_1(I/\tau_i)^{3/2}R$ where c_1 is a constant. The y intercept of this relation is set equal to 0, so that $P_r=0$ when $(I/\tau_i)^{3/2}R=0$. Assuming $P_r=c_1(I/\tau_i)^{3/2}R$, we obtain from the data a least-squares value of c_1, which is the value used for the plot. The curve plotted in Fig. 2(b) is obtained from Eq. (26) in a similar manner.

It is clear from Fig. 2 that the data are more consistent with ablation scaling [Eq. (14)] than RT scaling [Eq. (26)].

The fractional standard deviation of the difference between the observed x-ray powers plotted in Fig. 2(a) and the ablation-scaling relation [Eq. (14)] is $(13\pm2.3)\%$. For the wire-array configuration used to obtain the $R=10$ mm data plotted in this figure, the random 1σ shot-to-shot fluctuation in the peak radiated x-ray power is $(12\pm2.5)\%$ [29]. Hence the measurements plotted in Fig. 2(a) and the ablation-scaling relation [Eq. (14)] agree to within the inherent fluctuations in the pinch performance.

The $R=10$ mm data plotted in Fig. 2(a) are separated into two groups: one with $I\sim13$ MA and the other with $I\sim19$ MA. For both sets of measurements, τ_i was held constant at approximately 95 ns. As can be seen, Eq. (14) is consistent with the observed scaling of P_r with I. In addition, Fig. 2(a) suggests that to first order, Eq. (14) is consistent with the observed scaling of P_r with R.

The $\ell=10$ mm data appear to be less consistent with RT scaling [Eq. (26)]. As indicated by Fig. 2(b), most of the measured powers obtained at $R=10$ mm, $I\sim13$ MA are greater than the RT-scaling prediction; the powers obtained at $R=10$ mm, $I\sim19$ MA are less than the RT curve. The fractional standard deviation of the difference between the measurements plotted in Fig. 2(b) and the RT relation is

$(18\pm3.3)\%$. Figure 2(b) also suggests that Eq. (26) does not correctly predict the dependence of P_r on R.

In Fig. 3(a) we compare the 11 $\ell=20$ mm measurements [75,77,78] listed in Table I with Eq. (14); in Fig. 3(b), we compare the same measurements with Eq. (26). (We plot the $\ell=10$ mm and $\ell=20$ mm data separately, in Figs. 2 and 3, respectively, for reasons discussed in Sec. II C 2.) The theoretical curve plotted in Fig. 3(a) assumes that Φ and Γ are constant and that $P_r=c_2(I/\tau_i)^{3/2}R$ where c_2 is a constant. The y intercept of this relation is set equal to 0 so that $P_r=0$ when $(I/\tau_i)^{3/2}R=0$. Assuming $P_r=c_2(I/\tau_i)^{3/2}R$, we obtain from the data a least-squares value of c_2, which is the value used for the plot. The curve plotted in Fig. 3(b) is obtained from Eq. (26) in a similar manner.

As indicated by Fig. 3(a), these data are consistent with ablation scaling. The fractional standard deviation of the difference between the observed x-ray powers plotted in Fig. 3(a) and the ablation-scaling relation [Eq. (14)] is $(14\pm3.1)\%$. For the 7 measurements listed in Table I with $R=20$ mm and $\tau_i\sim105$ ns, the 1σ shot-to-shot fluctuation in the peak radiated x-ray power P_r is $(15\pm4.3)\%$. Hence, the measurements plotted in Fig. 3(a) and Eq. (14) agree to within the inherent fluctuations in the pinch performance.

The $\ell=20$ mm data are slightly less consistent with the RT model, as indicated by Fig. 3(b). The standard deviation of the difference between the measurements and the RT scaling [Eq. (26)] is $(16\pm3.5)\%$.

We note that of the 27 measurements listed in Table I and plotted in Figs. 2 and 3, the 7 measurements with the smallest values of the ratio $\delta_a/\delta_{\mathrm{RT}}$ [Eq. (31)] are those with $R=\ell=20$ mm, $m/\ell\sim2$ mg/cm, and $\tau_i\sim105$ ns. These 7 are plotted in Figs. 3(a) and 3(b). For these measurements, the quantity $(m/\ell)^{1/4}R^{-1/2}$ [given by Eq. (31)] is approximately 0.8, when m/ℓ is expressed in mg/cm and R in cm. Since the data plotted in Figs. 3(a) and 3(b) are not inconsistent with RT scaling, it is possible that for such values of $(m/\ell)^{1/4}R^{-1/2}$, RT effects are comparable to effects due to ablation. For all of the $R=10$ mm measurements plotted in Figs. 2(a) and 2(b), the quantity $(m/\ell)^{1/4}R^{-1/2}\geqslant1.3$.

2. Φ, Γ, *and the scaling of* E_r *with* ℓ

For the data plotted in each of Figs. 2(a) and 3(a), we assume that Φ and Γ are constant. This assumption is motivated by Eqs. (3) and (13), which indicate that Φ and Γ are weak functions of a/R when $a/R\ll1$. [For similar implosions, $F(r/R)$ is held constant, and Φ and Γ are functions only of a/R.] The experiments did not measure the quantities $F(r/R)$ or a/R, so this assumption cannot be directly validated.

However, we can use experimentally measured parameters to estimate Φ and Γ indirectly. We define the estimated quantities Φ_{expt} and Γ_{expt} as follows:

$$\Phi_{\mathrm{expt}}\equiv\frac{4\pi E_r}{\chi\mu_0\ell I^2},\tag{32}$$

$$\Gamma_{\mathrm{expt}}\equiv\frac{\tau_i I}{R}\left(\frac{\mu_0\ell}{2\pi m}\right)^{1/2},\tag{33}$$

where χ is a constant defined by $E_r=\chi E_k$. Equation (32) is obtained from Eqs. (2) and (3); Eq. (33) is identical to Eq. (13). Table I gives Φ_{expt} and Γ_{expt} for most of the shots listed. To obtain these estimates, the quantities on the right-hand sides of Eqs. (32) and (33) were obtained from the measurements listed in the table. We are interested here only in *relative* values of Φ_{expt} and to estimate these have arbitrarily set $\chi=1$.

As Table I makes evident, Γ_{expt} is, to within experimental uncertainties, constant for all of the measurements listed.

However, the mean value of Φ_{expt} for the $\ell=10$ mm data is a factor of 2 higher than the mean for the $\ell=20$ mm measurements. This observation confirms the length-scaling effect for E_r that is observed for experiments conducted on the Z accelerator, as discussed in Refs. [75,76]. It appears that to a good approximation, for conditions under which the experiments summarized in Table I were conducted, the total radiated x-ray energy E_r is independent of the axial pinch length ℓ. For this observation to be consistent with Eq. (15) requires that Φ change significantly as ℓ is changed.

An explanation for this effect is given in Refs. [75,76]: Since the change in the inductance of a pinch due to its implosion is a linear function of its length ℓ and since this change is greatest near the end of its implosion, the *current near the time of stagnation* is also a function of ℓ, even though the *peak current* may not change significantly as ℓ is varied. Hence, when ℓ is increased significantly, the value of $F(r/R)$ near stagnation (i.e., when r/R is small) decreases significantly, which as indicated by Eq. (3) results in a significant reduction in Φ. According to the 2D $(r-z)$ MHD simulations described in Ref. [76], this effect causes, for conditions of interest, E_r to be approximately independent of ℓ. (We caution, however, that the initial random-density perturbation of the simulations was changed as ℓ was changed, to improve the agreement with experiment [76].) For the results presented in Table I, E_r is independent of ℓ to within 2%.

The length-scaling effect can also be understood in terms of the initial inductance L of the radial-transmission-line system of the Z accelerator. This inductance is approximately 13 nH. The pinch is part of the radial system and contributes to its inductance as the pinch implodes. We label the time-dependent pinch inductance as $L_p(t)$ and define it such that $L_p(0)=0$. When $\ell=10$ mm, $L_p(\tau_i)=4.6$ nH (assuming a 10:1 pinch-radius convergence ratio). When $\ell=20$ mm, $L_p(\tau_i)=9.2$ nH. Since $L\sim L_p(\tau_i)$ when $\ell=20$ mm, the longer pinch causes a much greater change in the current near stagnation. Alternatively, we expect that the length-scaling effect can be neglected when $L\gg L_p(\tau_i)$.

Since the scaling relations developed in Secs. II A and II B assume that the implosions under consideration are similar [i.e., that $F(r/R)$ is held constant], we plot the $\ell=10$ mm and $\ell=20$ mm data separately (in Figs. 2 and 3, respectively) to maintain similarity.

We note that within each of these two groups, Φ_{expt} and Γ_{expt} are approximately constant, as is assumed for Figs. 2 and 3. For the $\ell=10$ mm data, Φ_{expt} is constant to within $\pm9.8\%$, and almost all of this variation can be accounted for by the $\pm9.1\%$ random shot-to-shot fluctuations in E_r [29]. (In Sec. II C 4, we present an additional discussion of Φ for the $\ell=10$ mm results.) Γ_{expt} is constant to $\pm2.3\%$; these variations are also primarily due to random experimental fluctua-

tions. For the $\ell=20$ mm data, Φ_{expt} is constant to within $\pm 14\%$ and Γ_{expt} to within $\pm 2.5\%$; both of these variations can be accounted for entirely by shot-to-shot fluctuations.

We also note that, according to Eqs. (3) and (13), Γ is a much weaker functional of $F(r/R)$ and a/R than is Φ. This is verified by Table I, which shows that even though the average value of Φ_{expt} changes by a factor of 2 when ℓ changes from 10 to 20 mm, the average value of Γ_{expt} changes by only 12%.

3. Optimum value of n

The ablation-dominated pinch model developed in Sec. II A assumes that the number of wires n is near the value that maximizes P_r. Hence any comparison between this model and experiment would require that the number of wires used for the measurements be near the optimum.

For the $R=10$ mm measurements listed in Table I, the number of wires n is 300, which is within the range that optimizes the peak-x-ray power as determined by Mazarakis and co-workers [25,27,28,33]. We caution, however, that the two $R=15$ mm experiments summarized in Table I, and plotted in Figs. 2(a) and 2(b), were performed with 220 wires, and that *direct* measurements have not yet been performed to determine the optimum range of n for the $R=15$ mm configuration. Hence it is likely that the two $R=15$ mm x-ray powers plotted in Figs. 2(a) and 2(b) would have been higher had the optimum number of wires been used. Additional experiments would be necessary to validate that the comparison presented in Figs. 2(a) and 2(b) between the two $R=15$ mm measurements and the scaling predictions are meaningful.

However, we have *indirect* experimental evidence that the $R=15$ mm results plotted in Fig. 2 are relevant. When $R=8.75$ mm and $\ell=20$ mm, Sanford and co-workers [79] find that increasing n from 120 to 240 increases the peak x-ray power by $(45\pm 22)\%$. When $R=20$ mm and $\ell=20$ mm, increasing n from 120 to 240 increases the power $(32\pm 22)\%$ [79]. When $R=10$ mm and $\ell=10$ mm, Mazarakis and colleagues find that increasing n from 120 to 240 increases the power $\sim 55\%$ [25,27,28,33]. Since these three ratios are, within experimental error, equivalent, the optimum range of n when $R=10$ mm and $\ell=10$ mm, which is 220–480, may be similar to the optimum ranges for the two configurations evaluated by Sanford *et al.* [79].

Assuming this is the case, we estimate from the results presented in [25,27,28,33] that the two $R=15$ mm x-ray-power measurements listed in Table I should be increased by $\sim 19\%$. These corrected powers would, on average, improve slightly the agreement between these two measurements and the predicted ablation scaling plotted in Fig. 2(a). These corrections would increase the *discrepancy* between these two measurements and the RT scaling plotted in Fig. 2(b).

The 4 measurements plotted in Figs. 3(a) and 3(b) with $\tau_i=127-169$ ns were taken with 480 wires [77]. The 7 measurements plotted in Figs. 3(a) and 3(b) with $\tau_i\sim 105$ ns were obtained with 240 wires [75,78]. Direct experiments have not yet been performed to determine the optimum range of n for the $R=20$ mm wire-array configuration used for these 11 shots, and would be necessary to validate that Figs. 3(a) and 3(b) are meaningful.

However, the indirect arguments presented above for the two $R=15$ mm measurements plotted in Figs. 2(a) and 2(b) suggest that the optimum range for n when $R=20$ mm may, in fact, be 220–480. If this is the case, we can use the results presented in [25,27,28,33] to estimate that the 4 measurements with $\tau_i=127-169$ ns plotted in Figs. 3(a) and 3(b) would have to corrected upward by 19%, and the 7 measurements with $\tau_i\sim 105$ ns would have to be increased by 13%. Such corrections would not significantly change the agreement between these measurements and the scaling relations plotted in Figs. 3(a) and 3(b).

4. Uncertainties in the x-ray-power scaling exponents

To estimate the uncertainties in the scaling exponents of Eq. (14), we consider the $\ell=10$ mm, $R=10$ mm measurements listed in Table I and plotted in Fig. 2(a). For these measurements the implosion time τ_i was held constant at ~ 95 ns [29]. (The quantities ℓ, R, and Γ were also held constant.) Neglecting the small variations of τ_i in this data, a least-squares analysis finds that the observed peak radiated x-ray power P_r and total radiated x-ray energy E_r scale with the peak pinch current I as follows [29]:

$$P_r \propto I^{1.24\pm 0.18}, \tag{34}$$

$$E_r \propto I^{1.73\pm 0.18}. \tag{35}$$

Equations (14), (15), (34), and (35) suggest that for these shots

$$\Phi \propto \frac{1}{I^{0.26\pm 0.18}}. \tag{36}$$

As indicated by Eq. (3), Φ is a function of a/R. When Γ is held constant, then according to Eqs. (17) and (21), a/R is a function of I, τ_i, and R. If Eq. (36) is correct when τ_i and R are constant, then, in general, we find from Eqs. (17) and (21) that

$$\Phi \propto \left(\frac{R}{a}\right)^{0.52\pm 0.36} \propto \left[\frac{R}{(I\tau_i)^{1/2}}\right]^{0.52\pm 0.36} \propto \frac{R^{0.52\pm 0.36}}{(I\tau_i)^{0.26\pm 0.18}}. \tag{37}$$

When Φ is given by Eq. (37) and Γ is constant, Eq. (14) can be expressed as

$$P_r \propto \frac{I^{1.24\pm 0.18}}{\tau_i^{1.76\pm 0.18}} R^{1.52\pm 0.36}\ell. \tag{38}$$

Consequently, for the conditions described in [29], Eq. (38) is the most likely expression for the scaling of P_r with I, τ_i, R, and ℓ. When both Φ and Γ are constant [as is assumed for Figs. 2(a) and 3(a)], Eq. (14) becomes instead

$$P_r \propto \left(\frac{I}{\tau_i}\right)^{3/2} R\ell. \tag{39}$$

The exponent of Eq. (36) is within 1.5σ of 0; hence the exponents of Eq. (38) are within 1.5σ of the exponents of

Eq. (39). Since this discrepancy is less than 2σ (the usual standard for determining whether a discrepancy is significant [80]), the difference between Eqs. (38) and (39) is *not* significant at a 95% confidence level. This is indicated graphically by Fig. 2(a), which shows that the data presented in Ref. [29] are consistent with Eq. (39) to within the shot-to-shot fluctuations in the measurements. Additional experiments conducted over a larger parameter regime, with improved statistics, would be required to reduce the uncertainties in the exponents.

However, there *is* a significant difference between Eq. (38) and RT scaling. When τ_i, R, and ℓ are held constant, Eq. (38) predicts that $P_r \propto I^{1.24\pm0.18}$ and Eq. (26) predicts $P_r \propto I^2$. Since the difference in these exponents is 4.2σ, it is highly unlikely that the wire array investigated in Ref. [29] follows RT scaling. This is illustrated by Fig. 2(b), which shows that the data of Ref. [29] are *not* consistent with Eq. (26).

III. THEORETICAL PINCH-ACCELERATOR-SYSTEM SCALING RELATIONS

A high-current z-pinch implosion is typically driven by a multimodule pulsed-power accelerator, with an architecture similar to that of the Z machine [34–42]. Each module of such an accelerator includes a pulse-forming section that delivers a forward-going electromagnetic power pulse to a constant-impedance transmission line. The lines in turn deliver power to an inductive radial-transmission-line system, which is located at the center of the accelerator and includes the z-pinch load. The radial-transmission-line system of the 20-MA Z accelerator is outlined in Fig. 4 [34–42]. Z has 36 pulsed-power modules that deliver power to its radial system [34–42]. Future accelerators, such as the 26-MA ZR machine, are expected to have a similar design [43–45].

In this section, we consider an accelerator that drives a single z-pinch load, and examine how the performance of such a system might be optimized. We begin by defining the x-ray-power efficiency η_x of such a coupled pinch-accelerator system, as follows:

$$\eta_x \equiv \frac{P_r}{P_a}, \tag{40}$$

where P_a is the peak electromagnetic power produced by the accelerator.

For this discussion we define P_a to be the peak power at the interface between the accelerator's modules and its radial-transmission-line system. (For the radial system outlined in Fig. 4, the interface is the insulator stack.) The electromagnetic power can be higher in the vacuum transmission line immediately upstream (within a few cm) of the z-pinch load, since an imploding pinch generates a voltage spike just before the pinch stagnates on axis. The power at the radial-system interface, however, is approximately equal to the number of modules multiplied by the forward-going power of each module, and is more representative of the capabilities and performance of the machine.

We estimate that for pinch-accelerator systems of interest, P_a scales as follows:

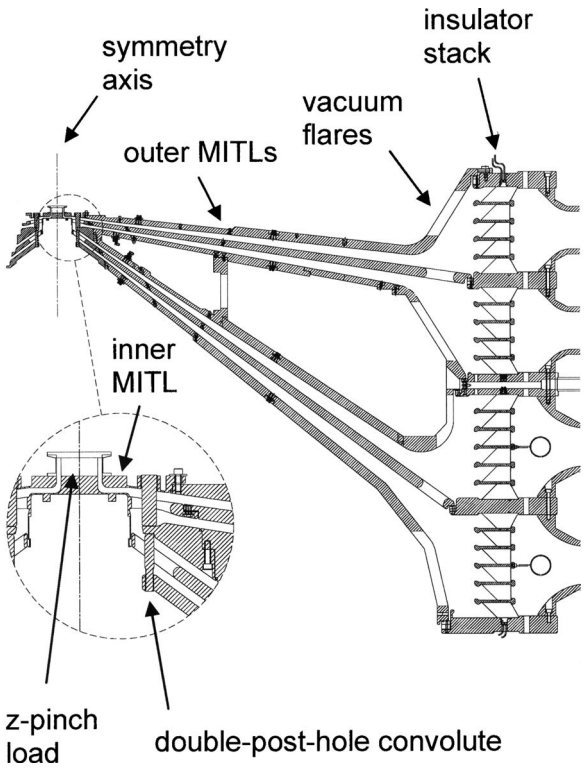

FIG. 4. The central radial-transmission-line system of the Z accelerator [34–42]. The outer diameter of the insulator stack is nominally 3.4 m. Everything located inside the insulator stack is operated under vacuum. The load illustrated here is a single wire-array z pinch.

$$P_a \propto VI, \tag{41}$$

where V is the peak voltage at the interface and I is the peak pinch current. (For this discussion, we assume that the pinch current is approximately equal to the current at the interface.) The peak energy E_a delivered by the accelerator to its radial system is proportional to the product $P_a\tau_i$:

$$E_a \propto P_a\tau_i \propto VI\tau_i. \tag{42}$$

For Eqs. (41) and (42) to be meaningful, the shapes of the voltage pulses $V(t)$ for the pinch-accelerator systems under consideration must be similar, where $V(t)$ is the time-dependent voltage at the interface. The shapes of the time-dependent current pulses $I(t)$ must also be similar, which has already been assumed for the discussion in Sec. II.

To estimate V we approximate $V(t)$ as

$$V(t) = L_r(t)\frac{dI(t)}{dt} + I(t)\frac{dL_r(t)}{dt}, \tag{43}$$

where $L_r(t)$ is the time-dependent radial-system inductance. The inductance $L_r(t)$ is a function of time primarily because of the imploding z pinch and can be expressed as

$$L_r(t) = L + L_p(t), \tag{44}$$

where L is the radial-system inductance at time $t=0$, and $L_p(t)$ is the time-dependent pinch inductance, which we de-

fine so that $L_p(0)=0$. The pinch inductance is greatest at stagnation, when $t=\tau_i$. When

$$L \gg L_p(\tau_i), \tag{45}$$

then V [the peak value of $V(t)$] is to a good approximation determined by the first term on the right-hand side of Eq. (43). [Equation (45) is also the condition required to minimize the pinch length-scaling effect discussed in Sec. II C 2.] When Eq. (45) is satisfied, Eqs. (43) and (44) can be combined to give

$$V \propto \left(\frac{LI}{\tau_i}\right). \tag{46}$$

Equation (46) assumes that the rise time of the current pulse is proportional to τ_i, which is valid for similar implosions.

As indicated by Fig. 4, the radial-transmission-line system of an accelerator such as Z consists of an insulator stack, vacuum flares, outer magnetically insulated vacuum transmission lines (MITL's), post-hole convolute, inner MITL, and z-pinch load [34–42]. As the current is increased in future accelerators above the levels achieved on Z, it will likely be necessary to increase the initial inductance L of the radial system to accommodate the correspondingly higher voltages at the insulator stack and other radial-system components.

Presently, these components and their associated technologies are subjects of active research, and it is not clear how the component designs will be optimized for currents significantly in excess of 26 MA. For example, the number of MITL levels and the radial-system diameter may increase from that of the Z machine. A review of the work in progress, and how it may affect the inductance of each component as the voltage is increased, is beyond the scope of this discussion.

However, we can make the following general observations. We can write

$$L = L_s + L_m + L_c, \tag{47}$$

where L_s is the inductance of the insulator stack and vacuum flares, L_m is the inductance of the outer MITL's, and L_c is the inductance of the post-hole convolute, inner MITL, and coaxial anode-cathode gap of the pinch [34–42]. These inductances will be affected by the two principal goals of the design of a radial system, which are (i) to minimize the probability of insulator-stack flashover [81] and (ii) to minimize damage to the MITL anodes due to deposition of MITL electron-flow current [35,37,42].

To estimate how the inductances will be affected, we consider radial systems for which the number of MITL levels and the outer radial-system diameter are held constant. (Similar arguments apply when these restrictions are lifted.) Assuming that the thickness of each insulator ring of the stack is at least a few cm thick, the electric field at which a single ring is expected to experience a surface flashover scales as [81]

$$E_{\text{flash}} \propto \left(\frac{V}{L_s}\right)_{\text{flash}} \propto t_{\text{eff}}^{-1/10}, \tag{48}$$

where t_{eff} is the effective pulse width of the voltage across the stack (as defined in Ref. [81]). Since the dependence on t_{eff} is weak, it will be necessary to increase L_s approximately linearly with V to keep the stack from flashing as the voltage is increased on future accelerators.

To estimate the scaling of the damage to the MITL anodes due to flow electrons [35,37,42], we consider a single MITL. We assume that the electron-flow current is a small fraction of the total current, which is the parameter regime of most interest. In this limit we have that [82–84]

$$V_m = Z_m(I_a^2 - I_k^2)^{1/2}, \tag{49}$$

where V_m is the peak MITL voltage, Z_m is the geometric vacuum impedance of the MITL, and I_a and I_k are the MITL anode and cathode currents at peak MITL voltage, respectively. When the flow current $I_f \equiv (I_a - I_k) \ll I_a$, we find from Eqs. (46), (47), and (49) that

$$Q_f \propto I_f \tau_i \propto \frac{V_m^2 \tau_i}{I_a Z_m^2} \propto \frac{(L_m + L_c)^2 V}{L_m^2 L} \propto \frac{V}{L} \propto \frac{V}{L_s + L_m + L_c}, \tag{50}$$

where Q_f is the electron-flow charge. Equation (50) assumes $L_m \propto Z_m$, $V_m \propto (L_m + L_c) I_a / \tau_i$, $I_a \propto I$, and that for conditions of interest, L_c scales approximately with L_m.

For radial systems similar to that of the Z accelerator, a significant fraction of Q_f is lost to the anode in the vicinity of the convolute and inner MITL [35,37,42] and damages the anodes of these components [37]. Hence it is desired to minimize Q_f. According to Eq. (50), to keep Q_f constant as V is increased requires that $(L_m + L_c) \propto L_s \propto V$—i.e., that $L \propto V$. However [as indicated by Eq. (46)] this would require holding I/τ_i constant, which for an ablation-dominated pinch would, to a good approximation, hold P_r constant [as indicated by Eq. (14)]. Since L_s must scale approximately as V, it appears that we can increase $L_m + L_c$, and hence L, only as sublinear functions of V, and in general be forced to accept larger values of Q_f as the voltage is increased on future accelerators.

Consequently, the total radial-system inductance L will likely increase as V is increased on future accelerators. For definiteness, we consider here accelerators for which L scales approximately as a power-law function of V:

$$L \propto V^{\beta}. \tag{51}$$

When $\beta = 2/5$, Eq. (51) is consistent to first order with the radial-system designs of the Saturn ($I = 8$ MA, $\tau_i \sim 45$ ns), Z ($I = 20$ MA, $\tau_i \sim 100$ ns), and ZR ($I = 26$ MA, $\tau_i \sim 100$ ns) accelerators.

Combining Eqs. (41), (42), (46), and (51), and assuming $\beta = 2/5$, we obtain the following relations:

$$P_a \propto \frac{I^{8/3}}{\tau_i^{5/3}}, \tag{52}$$

$$E_a \propto \frac{I^{8/3}}{\tau_i^{2/3}}, \tag{53}$$

$$V \propto \left(\frac{I}{\tau_i}\right)^{5/3}, \tag{54}$$

$$L \propto \left(\frac{I}{\tau_i}\right)^{2/3}. \tag{55}$$

Equations (52)–(55) give P_a, E_a, V, and L as functions of I and τ_i and are valid when Eq. (45) is applicable.

Assuming that the accelerator is coupled to an ablation-dominated pinch and that Φ and Γ are held constant, we combine Eqs. (14), (40), and (52)–(55) to obtain the following relations:

$$P_a \propto \tau_i \left(\frac{P_r}{R\ell}\right)^{16/9}, \tag{56}$$

$$E_a \propto \tau_i^2 \left(\frac{P_r}{R\ell}\right)^{16/9}, \tag{57}$$

$$V \propto \left(\frac{P_r}{R\ell}\right)^{10/9}, \tag{58}$$

$$L \propto \left(\frac{P_r}{R\ell}\right)^{4/9}, \tag{59}$$

$$\eta_x \equiv \frac{P_r}{P_a} \propto \frac{1}{\tau_i}\left[\frac{(R\ell)^{16/9}}{P_r^{7/9}}\right]. \tag{60}$$

These expressions give P_a, E_a, V, L, and η_x as functions of P_r, τ_i, R, and ℓ, and are valid when Eq. (45) applies. As noted above, Eqs. (56)–(60) assume that the pinch is ablation dominated; a different set of expressions is obtained when an x-ray-power scaling relation other than Eq. (14) is assumed.

As indicated by Eqs. (56) and (60), when the product $R\ell$ is held constant, the accelerator power P_a required to achieve a given value of P_r is proportional to τ_i. According to Eq. (57), the requisite accelerator energy E_a is proportional to τ_i^2. Hence considerably less accelerator power and energy are required to achieve a given value of P_r when τ_i is decreased. [According to Eqs. (58) and (59), the requisite values of V and L are independent of τ_i.] We note that although Eqs. (56)–(60) assume $\beta=2/5$, the exponents of τ_i in these five relations are independent of β.

IV. THEORETICAL SCALING RELATIONS FOR A COUPLED CAPSULE-HOHLRAUM-ACCELERATOR SYSTEM

The previous section develops scaling relations for the accelerator parameters required to achieve a given value of P_r. Using these results, we develop below scaling relations for the parameters required to achieve the values of P_r and τ_w that would be necessary to realize high-yield ICF. For this discussion, we consider an accelerator that drives the implosion of two wire-array z pinches in a double-pinch-driven hohlraum system, as indicated in Fig. 1. We assume that the hohlraum radiation in turn drives the implosion of an ICF fuel capsule [1–12] and that the capsule design is similar to that detailed in Fig. 5.

FIG. 5. (Color) Cross-sectional view of the base-line ICF capsule design developed by Vesey *et al.* [11,12]. The outer radius of the ablator R_c=2.65 mm, the outer radius of the DT-ice layer R_f =2.46 mm, and the inner radius of the ice is 2.18 mm. (This figure is a detail of the capsule illustrated in Fig. 1). Performance parameters for this capsule are listed in Table II.

We begin by defining the thermonuclear-yield efficiency of a coupled capsule-hohlraum-accelerator system as follows:

$$\eta_y \equiv \frac{E_y}{E_a}, \tag{61}$$

where E_y is the total thermonuclear yield and E_a is as defined in Sec. III. The quantity η_y is an upper bound on the system efficiency, since η_y does not account for the efficiency of the transfer of energy from the accelerator's Marx generators to the radial-transmission-line system.

We limit our discussion to systems with capsule implosions that are hydrodynamically similar, for which the initial deuterium-tritium (DT) fuel density ρ_0, initial fuel aspect ratio ζ, and peak drive pressure applied to the outer fuel surface P_f are held constant [85]. The initial fuel aspect ratio is defined by

$$\zeta \equiv \frac{R_f}{\Delta R_f}, \tag{62}$$

where R_f is the initial outer radius of the DT-fuel (ice) layer and ΔR_f is the initial radial thickness of the ice [85,86]. (The

ice layer is illustrated in Fig. 5.) As discussed in Ref. [85], for such implosions α_{if}, IFAR, v_c, and the fuel convergence ratio are also held constant. (The quantity α_{if} is the ratio of the pressure in the capsule's DT fuel at a given density to the Fermi degeneracy pressure and is evaluated when the fuel is in flight [86,87], IFAR is the fuel's in-flight aspect ratio [86,87], and v_c is the peak fuel implosion velocity.)

For such implosions and for sufficiently large capsules, we expect that E_y scales approximately as follows:

$$E_y \propto m_f \propto \frac{\rho_0 R_c^3}{\zeta}, \tag{63}$$

where m_f is the fuel mass (i.e., the mass of the capsule's DT-ice layer) and R_c is the outer capsule radius. Equation (63) assumes $\zeta \gg 1$ and $R_f \propto R_c$. For the capsules considered in this article, Eq. (63) is consistent to first order with 1D LASNEX simulations [12].

To determine the conditions under which P_f is held constant, we assume that for capsules under consideration

$$P_f \propto P_c, \tag{64}$$

where P_c is the peak ablation pressure at the outer capsule (ablator) surface. We also assume [87]

$$P_c \propto T_r^{3.5}, \tag{65}$$

where T_r is the peak temperature of the hohlraum radiation incident upon the capsule.

For an *idealized* double-pinch-driven hohlraum, T_r is given approximately by Eq. (42) of Ref. [26]:

$$[(1-\alpha_w)A_w + A_h + (1-\alpha_g)A_g]\sigma T_r^4 = 2P_r. \tag{66}$$

In this expression A_w is the area of the hohlraum wall excluding the area of the two pinches, α_w is the albedo of area A_w, A_h is the area of holes in the wall, A_g is the area of the anode-cathode (AK) gaps of the two pinches, α_g is the albedo of the gaps [3,88,89], and σ is the Stefan-Boltzmann constant. (As indicated in Fig. 1, there is an AK gap at the base of each of the two pinches.) Equation (66) makes the simplifying assumptions that the capsule area can be neglected and that the *net* power radiated by the two pinches [as defined by Eq. (7) of Ref. [26]] equals $2P_r$. Assuming

$$A_g \propto A_w \tag{67}$$

and $A_h = 0$, we approximate Eq. (66) as

$$\sigma T_r^4 = \frac{2P_r}{(1-\alpha_{\text{eff}})A_w}, \tag{68}$$

where α_{eff} is an effective system albedo.

According to Rosen [90] and Lindl *et al.* [91], the time-dependent albedo of a gold wall satisfies

$$1 - \alpha_{\text{gold}} \propto T_r^{-0.7} \tau_w^{-0.38}, \tag{69}$$

where τ_w is the width of the radiation pulse. Assuming that the scaling indicated by Eq. (69) applies to $(1-\alpha_{\text{eff}})$, we combine Eqs. (68) and (69) to obtain

$$T_r^{3.3} \propto \frac{P_r \tau_w^{0.38}}{A_w}, \tag{70}$$

which is similar to expressions developed by Cuneo *et al.* in Ref. [3]. Consequently, according to Eqs. (64) and (65), to hold P_f constant requires that T_r, and hence the expression on the right-hand side of Eq. (70), be held constant.

We further limit our discussion to hohlraum systems that have similar radiation geometries—i.e., for which

$$A_g \propto A_w \propto R^2 \propto \ell^2 \propto R_c^2, \tag{71}$$

where R and ℓ are the initial pinch radius and axial length, respectively, as defined in Fig. 1 and Sec. II A. For such systems the uniformity of the hohlraum radiation incident upon the capsule is held constant.

To complete the system of equations, we observe that for similar capsule implosions, the capsule-implosion time τ_c is proportional to τ_w, the effective pulse width of the x-ray-power radiated by the pinch:

$$\tau_c \propto \frac{R_c}{v_c} \propto \tau_w. \tag{72}$$

In addition, we consider in this article two other capsule parameters of interest: the hohlraum-radiation energy absorbed by the capsule E_c and the ignition margin M. E_c scales as follows:

$$E_c \propto (T_r^4 R_c^2)\tau_c \propto \frac{T_r^4 R_c^3}{v_c}. \tag{73}$$

The scaling of M is given by Eq. (A5) in the Appendix.

Since for systems under consideration the parameters ρ_0, ζ, T_r, α_{if}, and v_c are held constant, we find from Eqs. (19), (63), (70)–(73), and (A5) that

$$E_y \propto R_c^3, \tag{74}$$

$$E_c \propto R_c^3, \tag{75}$$

$$M \propto R_c^{0.64}, \tag{76}$$

$$P_r \propto R_c^{1.62}, \tag{77}$$

$$E_r \propto R_c^{2.62}, \tag{78}$$

$$\tau_w \propto R_c, \tag{79}$$

$$A_w^{1/2} \propto A_g^{1/2} \propto R \propto \ell \propto R_c. \tag{80}$$

Assuming an ablation-dominated pinch and that Φ and Γ are held constant, we combine Eqs. (14)–(21), (56)–(61), and (74)–(80) to obtain the following scaling relations for a coupled capsule-hohlraum-accelerator system:

$$R_c \propto I^{1.23} \propto \tau_i^{0.94}, \tag{81}$$

$$E_y \propto R_c^3 \propto I^{3.70} \propto \tau_i^{2.82}, \tag{82}$$

$$E_c \propto R_c^3 \propto I^{3.70} \propto \tau_i^{2.82}, \tag{83}$$

$$M \propto R_c^{0.64} \propto I^{0.79} \propto \tau_i^{0.60}, \tag{84}$$

$$P_r \propto R_c^{1.62} \propto I^2 \propto \tau_i^{1.52}, \tag{85}$$

$$E_r \propto R_c^{2.62} \propto I^{3.23} \propto \tau_i^{2.46}, \tag{86}$$

$$\tau_w \propto R_c \propto I^{1.23} \propto \tau_i^{0.94}, \tag{87}$$

$$A_w^{1/2} \propto A_g^{1/2} \propto R \propto \ell \propto R_c \propto I^{1.23} \propto \tau_i^{0.94}, \tag{88}$$

$$I \propto R_c^{0.81} \propto \tau_i^{0.76}, \tag{89}$$

$$\frac{m}{\ell} \propto R_c^{1.75} \propto I^{2.16} \propto \tau_i^{1.64}, \tag{90}$$

$$\frac{a}{R} \propto \frac{1}{R_c^{0.06}} \propto \frac{1}{I^{0.08}} \propto \frac{1}{\tau_i^{0.06}}, \tag{91}$$

$$P_a \propto R_c^{0.39} \propto I^{0.48} \propto \tau_i^{0.36}, \tag{92}$$

$$E_a \propto R_c^{1.45} \propto I^{1.79} \propto \tau_i^{1.36}, \tag{93}$$

$$V \propto \frac{1}{R_c^{0.42}} \propto \frac{1}{I^{0.52}} \propto \frac{1}{\tau_i^{0.40}}, \tag{94}$$

$$L \propto \frac{1}{R_c^{0.17}} \propto \frac{1}{I^{0.21}} \propto \frac{1}{\tau_i^{0.16}}, \tag{95}$$

$$\eta_x \propto R_c^{1.23} \propto I^{1.52} \propto \tau_i^{1.16}, \tag{96}$$

$$\eta_y \propto R_c^{1.55} \propto I^{1.91} \propto \tau_i^{1.46}. \tag{97}$$

As indicated by Eqs. (85), (86), (89), (92), and (93), increasing τ_i increases the values of P_r, E_r, I, P_a, and E_a required to achieve high yield. However, the requisite values of V and L *decrease* as τ_i is increased [Eqs. (94) and (95)]. Furthermore, the x-ray power and thermonuclear-yield efficiencies η_x and η_y are *increasing* functions of τ_i [Eqs. (96) and (97)].

According to Eq. (60) of Sec. III, when R and ℓ are held constant, η_x *decreases* as τ_i is increased. Equation (96) predicts instead that η_x *increases* with τ_i, because Eq. (96) assumes that R and ℓ scale with R_c, I, and τ_i according to Eq. (88). Such scaling can be assumed only when $L \gg L_p(\tau_i)$—i.e., when the pinch length-scaling effect discussed in Sec. II C 2 can be neglected.

As noted above, Eqs. (81)–(97) assume that the pinch is ablation dominated and that Φ and Γ are held constant. To develop a similar set of equations assuming Eq. (38) would require combining Eqs. (15)–(21), (37), (38), (40), (52)–(55), (61), and (74)–(80). For RT scaling, one would use Eqs. (26)–(30), (40), (52)–(55), (61), and (74)–(80).

V. ESTIMATED REQUIREMENTS FOR z-PINCH-DRIVEN HIGH-YIELD ICF

Vesey and colleagues [11,12] have recently developed a base-line ICF capsule design for the double-pinch-driven hohlraum. The design is outlined in Fig. 5. Several performance parameters of this design have been determined from 1D LASNEX simulations [11,12] and are listed in Table II.

TABLE II. Parameters of the base-line ICF capsule design developed by Vesey *et al.* [11,12]. The capsule is illustrated in Fig. 5. The scaling relations presented in Sec. IV assume that ζ, T_r, α_{if}, IFAR, v_c, and the fuel convergence ratio are held constant.

Initial outer capsule radius R_c	2.65 mm
Ablator constituents	Be+0.2 at. %Cu
Initial outer DT-ice radius R_f	2.46 mm
Initial inner DT-ice radius	2.18 mm
Initial DT-ice aspect ratio ζ	8.79
Density of the DT fill gas	0.0003 g/cm^3
Peak drive temperature T_r	223 eV
In-flight fuel adiabat α_{if}	0.74
In-flight fuel aspect ratio IFAR	34
Peak fuel implosion velocity v_c	2.6×10^7 cm/s
Fuel convergence ratio	34
Energy absorbed by the capsule E_c	1.41 MJ
1D LASNEX thermonuclear yield E_y	528 MJ
Ignition margin M	1.35
Remaining fuel kinetic energy at ignition f_{ke} (as a fraction of the peak kinetic energy)	26%

Assuming this design, we estimate the radiation, pinch, and accelerator parameters that would be required to achieve high-yield fusion ($E_y \sim 0.4$ GJ). We also estimate the parameters required to drive a larger capsule to achieve a thermonuclear yield in excess of 3 GJ for inertial-fusion-energy research [13,14]. The estimated parameters are listed in Tables III and IV. The estimates are given for three scaling relations of the peak pinch x-ray power P_r.

Table III lists the requisite radiation, pinch, and accelerator parameters assuming that the anode-cathode gap of the pinch is 2 mm when $R=\ell=10$ mm [1,11,12]. Recent experiments suggest that gaps larger than 2 mm may be necessary at the pinch currents required to achieve high yield [29]. A $R=\ell=10$ mm hohlraum system with a gap larger than 2 mm would be less efficient (since a larger gap would act as a larger radiation sink) and consequently would require a higher x-ray power to achieve the same radiation temperature. Presently it is not clear what the necessary gaps will be at the higher currents. Hence to determine the *sensitivity* of the various parameters to the width of the gap, we present in Table IV estimates of these parameters assuming that the gap is 4 mm when $R=\ell=10$ mm. Both Tables III and IV assume that the gap is proportional to R and ℓ [i.e., that $A_g^{1/2} \propto R \propto \ell$, as required by Eq. (88)].

We caution that, in this article, we discuss only our present best estimates of the various parameters that would be required to achieve high yield, and do not address many issues that would need to be considered in a complete study. For example, we assume that the calculated wall albedos [11,12] implicit in the P_r requirements listed in Tables III and IV are correct; i.e., we do not explore possible inaccuracies in LASNEX. In addition, we do not consider to what

TABLE III. Estimated capsule, radiation, pinch, and accelerator parameters required to achieve 0.53 and 3.2 GJ thermonuclear yields. The radiation, pinch, and accelerator parameters assume that the anode-cathode gap of the pinch is 2 mm when $R=\ell=10$ mm, and that the gap is proportional to R and ℓ. (Table IV lists parameters assuming that the gap is 4 mm when $R=\ell=10$ mm.) We assume that the accelerator drives a double-pinch-driven hohlraum, that in turn drives the implosion of an ICF fuel capsule. The parameters are given for three x-ray-power P_r scaling relations. Capsule parameters are listed in columns 2–5: R_c is the initial capsule radius, E_y is the 1D thermonuclear yield, E_c is the radiation energy absorbed by the capsule during its implosion, and f_{ke} the fractional remaining fuel kinetic energy at ignition. Radiation parameters are listed in columns 6–8: P_r is the total peak x-ray power radiated by the two pinches in the double-pinch-driven hohlraum, τ_w is the x-ray-power pulse width [as defined by Eq. (19)], R is the initial pinch radius, and ℓ is the axial length of each pinch. Pinch parameters are listed in columns 9–11: I is the peak current in each pinch, τ_i is the pinch implosion time, and m/ℓ is the pinch mass per unit length. Accelerator parameters are listed in columns 12–15: P_a is the *total* accelerator power at the input to the accelerator's two radial transmission-line systems, E_a is the *total* accelerator energy delivered to the two radial systems, V is the voltage at the input to the radial systems, and L is the initial inductance of each radial system. (The accelerator parameters assume that two radial systems feed current to the double-pinch-driven hohlraum, one for each pinch, as suggested by Fig. 1.) The pinch and accelerator parameters assume $L \gg L_p(\tau_i)$—i.e., that the pinch length-scaling effect discussed in Sec. II C 2 can be neglected.

P_r scaling	R_c (mm)	E_y (GJ)	E_c (MJ)	f_{ke}	P_r (TW)	τ_w (ns)	R, ℓ (mm)	I (MA)	τ_i (ns)	m/ℓ (mg/cm)	P_a (TW)	E_a (MJ)	V (MV)	L (nH)
$P_r \propto \frac{I^2}{\tau_i}\ell$	2.65	0.53	1.4	26%	1800	10.1	10.0	42	91	26	988	57	13	23
	4.82	3.2	8.5	49%	4750	18.4	18.2	69	166	69	1330	139	10	21
$P_r \propto \left(\frac{I}{\tau_i}\right)^{3/2} R\ell$	2.65	0.53	1.4	26%	1800	10.1	10.0	42	63	12	1860	73	24	29
	4.82	3.2	8.5	49%	4750	18.4	18.2	69	118	35	2350	175	18	26
$P_r \propto \frac{I^{1.24}}{\tau_i^{1.76}} R^{1.52}\ell$	2.65	0.53	1.4	26%	1800	10.1	10.0	47	60	14	2640	100	30	32
	4.82	3.2	8.5	49%	4750	18.4	18.2	76	114	40	3210	232	23	29

extent the peak x-ray powers would have to be increased above the values presented here to counter effects due to shot-to-shot fluctuations in the pinch radiation [29,79,92]. Furthermore, we do not address capsule-implosion instabilities, radiation-pulse-shaping requirements, cryogenic requirements (such as temperature uniformity), capsule-preheat issues, issues related to plasma fill of the hohlraum, issues having to do with the fabricability of the various capsule and wire-array components, shot-rate requirements, etc. The results presented here are intended to serve as first approximations and are valid only if the calculated wall albedos implicit in the P_r requirements are correct, and if the various issues not considered can be neglected.

A. Capsule parameters

The $R_c=2.65$ mm capsule assumed for Tables III and IV is the design developed by Vesey *et al.* [11,12]. The $R_c=4.82$ mm capsule is a scaled version of the 2.65-mm design; the capsule dimensions have been increased a factor of 1.82 to increase both E_c and E_y a factor of 6. As discussed in Sec. IV and the Appendix, the scaling relations we assume hold constant the parameters ζ, T_r, α_{if}, IFAR, v_c, and the capsule convergence ratio at the values listed in Table II. We also hold constant the uniformity of the radiation incident on the capsule, since as discussed in Sec. IV we assume $A_w^{1/2} \propto A_g^{1/2} \propto R \propto \ell \propto R_c$.

The thermonuclear yield E_y listed in Tables III and IV when $R_c=4.82$ mm assumes that when $R_c=2.65$ mm, $E_y=528$ MJ (as indicated in Table II), and that E_y scales according to Eq. (74). The absorbed capsule energy E_c and fractional remaining kinetic energy f_{ke} for the $R_c=4.82$ mm capsule are obtained in a similar manner, assuming Eqs. (75), (76), (A5), and (A6).

B. Radiation parameters

According to the LASNEX simulations performed by Vesey *et al.* [11,12], the peak x-ray power P_r required to achieve the capsule performance parameters listed in Table II is 900 TW per pinch (1800 TW total). This assumes that the x-ray-power pulse width τ_w [as defined by Eq. (19)] is 10.1 ns. This also assumes the double-pinch-hohlraum geometry described by Hammer *et al.* in Ref. [1]—i.e., that $R=\ell=10$ mm and that the anode-cathode gap of the pinch is 2 mm. When the gap is 4 mm (and $R=\ell=10$ mm), Vesey *et al.* [11,12] find that the requisite values of P_r and τ_w are 1290 TW per pinch and 10.1 ns, respectively.

These are the peak power and pulse width requirements when $R_c=2.65$ mm and $R=\ell=10$ mm. The requisite values of P_r, τ_w, R, and ℓ for the $R_c=4.82$ mm capsule are obtained by scaling from the requirements at $R_c=2.65$ mm, assuming Eqs. (77), (79), and (80).

C. Pinch parameters

The pinch parameters required to drive the $R_c=2.65$ mm and $R_c=4.82$ mm capsules are given in Tables III and IV for three different x-ray-power scaling relations. The results presented assume that for all cases considered $L \gg L_p(\tau_i)$—i.e., that the pinch length-scaling effect discussed in Sec. II C 2 can be neglected.

TABLE IV. Estimated capsule, radiation, pinch, and accelerator parameters required to achieve 0.53 and 3.2 GJ thermonuclear yields. The radiation, pinch, and accelerator parameters assume that the anode-cathode gap of the pinch is 4 mm when $R=\ell=10$ mm, and that the gap is proportional to R and ℓ. (Table III lists parameters assuming that the gap is 2 mm when $R=\ell=10$ mm.) We assume that the accelerator drives a double-pinch-driven hohlraum, that in turn drives the implosion of an ICF fuel capsule. The parameters are given for three x-ray-power P_r scaling relations. Capsule parameters are listed in columns 2–5: R_c is the initial capsule radius, E_y is the 1D thermonuclear yield, E_c is the radiation energy absorbed by the capsule during its implosion, and f_{ke} the fractional remaining fuel kinetic energy at ignition. Radiation parameters are listed in columns 6–8: P_r is the total peak x-ray power radiated by the two pinches in the double-pinch-driven hohlraum, τ_w is the x-ray-power pulse width [as defined by Eq. (19)], R is the initial pinch radius, and ℓ is the axial length of each pinch. Pinch parameters are listed in columns 9–11: I is the peak current in each pinch, τ_i is the pinch implosion time, and m/ℓ is the pinch mass per unit length. Accelerator parameters are listed in columns 12–15: P_a is the *total* accelerator power at the input to the accelerator's two radial transmission-line systems, E_a is the *total* accelerator energy delivered to the two radial systems, V is the voltage at the input to the radial systems, and L is the initial inductance of each radial system. (The accelerator parameters assume that two radial systems feed current to the double-pinch-driven hohlraum, one for each pinch, as suggested by Fig. 1.) The pinch and accelerator parameters assume $L \gg L_p(\tau_i)$—i.e, that the pinch length-scaling effect discussed in Sec. II C 2 can be neglected.

P_r scaling	R_c (mm)	E_y (GJ)	E_c (MJ)	f_{ke}	P_r (TW)	τ_w (ns)	R, ℓ (mm)	I (MA)	τ_i (ns)	m/ℓ (mg/cm)	P_a (TW)	E_a (MJ)	V (MV)	L (nH)
$P_r \propto \frac{I^2}{\tau_i}\ell$	2.65	0.53	1.4	26%	2580	10.1	10.0	51	91	38	1600	92	17	26
	4.82	3.2	8.5	49%	6810	18.4	18.2	82	166	99	2150	225	14	24
$P_r \propto \left(\frac{I}{\tau_i}\right)^{3/2} R\ell$	2.65	0.53	1.4	26%	2580	10.1	10.0	51	59	16	3320	124	35	34
	4.82	3.2	8.5	49%	6810	18.4	18.2	82	111	44	4190	295	27	31
$P_r \propto \frac{I^{1.24}}{\tau_i^{1.76}} R^{1.52}\ell$	2.65	0.53	1.4	26%	2580	10.1	10.0	57	56	18	4980	177	46	38
	4.82	3.2	8.5	49%	6810	18.4	18.2	92	107	52	6060	410	35	34

The first relation listed in Tables III and IV [$P_r \propto (I^2/\tau_i)\ell$] is applicable to an idealized RT-dominated pinch [Eq. (26)] and is the most optimistic of the three. The second [$P_r \propto (I/\tau_i)^{3/2} R\ell$] assumes an idealized ablation-dominated pinch [Eq. (14)] and that Φ and Γ are constant. This relation is an upper bound on what is achievable for an ablation-dominated array. The third [$P_r \propto (I^{1.24}/\tau_i^{1.76}) R^{1.52}\ell$] is given by Eq. (38). The difference between the second and third relations is indicative of the present uncertainties in the exponents of Eq. (14), as discussed in Sec. II C 4. Hence the differences in the pinch and accelerator parameters given for the second and third P_r scaling relations indicate the present level of uncertainties in these parameters.

To estimate the requisite values of I, τ_i, and m/ℓ listed in Tables III and IV, we assume that for all three P_r scaling relations, $P_r=82$ TW (per pinch) and $\tau_w=10.5$ ns when $I=13$ MA, $\tau_i=95$ ns, $m/\ell=2.68$ mg/cm, and $R=\ell=10$ mm, as observed experimentally [29]. We also assume that the wire-array-pinch material is tungsten and that the initial tungsten mass density is held constant. In addition, we assume that $F(r/R)$ is the same as it was for the experiments described in Ref. [29].

To obtain the estimates of I, τ_i, and m/ℓ for the relation $P_r \propto (I^2/\tau_i)\ell$, we normalize Eqs. (26), (28), and (30) to the $I=13$ MA experimental results [29]. To obtain the estimates for the relation $P_r \propto (I/\tau_i)^{3/2} R\ell$, we use instead Eqs. (14), (16), (18), and (20), assuming that Φ and Γ are held constant. When $P_r \propto (I^{1.24}/\tau_i^{1.76}) R^{1.52}\ell$, we use Eqs. (16), (18), (20), and (38) and assume Γ is constant.

As indicated in Fig. 1, the anode of each pinch in a double-pinch-driven hohlraum includes a fairly open set of beryllium spokes [1–12]. For the estimates listed in Tables III and IV, we assume that the peak x-ray power achieved from a pinch with such spokes is the same as that obtained when the spokes are replaced with a flat solid electrode, as was used for the experiments described in Ref. [29]. Preliminary experiments on Z suggest that the spokes do not significantly affect the x-ray emission [4]. The results presented in Tables III and IV assume the spokes have no effect.

In addition to the pinch parameters listed in Tables III and IV, we have also estimated the requisite values of a/R, assuming $a/R=0.10$ when $I=13$ MA, $\tau_i=95$ ns, $m/\ell=2.68$ mg/cm, and $R=\ell=10$ mm. Under these conditions, we find from Eq. (29) that $a/R=0.10$ for all of the systems considered in Tables III and IV that assume $P_r \propto (I^2/\tau_i)\ell$. For the systems listed in Tables III and IV that assume either $P_r \propto (I/\tau_i)^{3/2} R\ell$ or $P_r \propto (I^{1.24}/\tau_i^{1.76}) R^{1.52}\ell$, we use Eqs. (17) and (21) to estimate that a/R varies between 0.14 and 0.16.

D. Accelerator parameters

To obtain the estimates of P_a, E_a, V, and L listed in Tables III and IV, we assume $P_a=55$ TW, $E_a=3.3$ MJ, $V=3.1$ MV, and $L=13$ nH, when $I=19$ MA and $\tau_i=95$ ns, and normalize Eqs. (52)–(55) to these values. These values of P_a, E_a, and V were measured on the Z accelerator for the experiments described in Ref. [29]. The measurements were performed with the power-flow-diagnostic package described in Ref. [93]. We use these values of P_a, E_a, and V because they have been obtained at $L=13$ nH, which is the smallest inductance that can presently be used to obtain reliable accelerator operation when $I=19$ MA and $\tau_i=95$ ns.

The accelerator parameters P_a, E_a, V, and L listed in Tables III and IV assume that two vacuum transmission lines feed current to the double-pinch-driven hohlraum system, one line for each pinch, as indicated in Fig. 1 [1,11,12]. In such a double-feed configuration, the two pinches are connected electrically in parallel. Two radial transmission-line systems (each of which would resemble the system illustrated in Fig. 4) would be needed to drive two such pinches, one system for each pinch. It is also possible to connect the two pinches in series and drive them from one side. At first it might appear that a single-sided drive would require significantly less accelerator power. However, the hohlraum of a single-sided system is substantially less efficient [3], and it is presently not clear which approach would be more economical. Hence for this article we assume a double-sided configuration, since this appears to be the more conservative approach. Tables III and IV give the current and inductance *per pinch*, since a double-sided pinch-accelerator system can be considered as consisting of two accelerators in parallel, one for each pinch. However, the values of P_a and E_a listed in Tables III and IV are the *total* requisite values.

As indicated by Eqs. (92) and (93) and Tables III and IV, the values of P_a and E_a required to achieve high-yield fusion decrease as the implosion time τ_i is decreased. For example, when $P_r \propto (I/\tau_i)^{3/2} R\ell$, Eqs. (92) and (93) suggest that reducing the implosion time from 120 to 59 ns would reduce the requisite values of P_a and E_a by factors of 1.3 and 2.6, respectively. However, the x-ray-power and thermonuclear-yield efficiencies η_x and η_y are *increasing* functions of τ_i, and the requisite values of V and L *decrease* as τ_i is increased.

We also find that the three P_r scaling relations considered in Tables III and IV have significantly different accelerator requirements. For example, the requisite values of P_a for a given thermonuclear yield are a factor of 2.4–3.1 less for RT scaling $[P_r \propto (I^2/\tau_i)]$ than when $P_r \propto (I^{1.24}/\tau_i^{1.76}) R^{1.52} \ell$. The requisite values of E_a are a factor of 1.7–1.9 less.

In addition, we find that the requisite values P_a and E_a are strong functions of the anode-cathode gap of the pinch. As indicated by Tables III and IV, increasing the gap from 2 to 4 mm when $R=\ell=10$ mm increases P_a and E_a by factors of 1.6–1.9 and 1.6–1.8, respectively.

E. Capsule-hohlraum-accelerator scaling relations

Equations (81)–(97) give the scaling of various parameters (required to achieve fusion yields > 0.4 GJ) for a coupled capsule-hohlraum-accelerator system assuming $P_r \propto (I/\tau_i)^{3/2} R\ell$. The third rows of Tables III and IV give parameters assuming $P_r \propto (I/\tau_i)^{3/2} R\ell$ and $R_c = 2.65$ mm. Equations (81)–(97) can be used to scale from these results to other values of R_c. Equivalently [as indicated by Eqs. (81)–(97)], the scaling can be performed using either I or τ_i. As discussed in Sec. IV, expressions similar to Eqs. (81)–(97) can be readily developed for the other P_r scaling relations.

VI. DISCUSSION

Given the complex three-dimensional time-dependent nature of the ablation, implosion, and stagnation processes, the pinch scaling relations presented in Secs. II A and II B can be accurate to at most first order ($\sim 10-20\%$). In addition, the comparison in Sec. II C between the relations and measurements is not definitive, because of the limited parameter regime accessed by the experiments. Furthermore, the apparently random shot-to-shot fluctuations inherent in the x-ray power radiated by a pinch [29,79,92] reduce the precision of these comparisons. Additional experiments would be needed to validate Eqs. (14)–(21) and (26)–(30) over their respective regimes of applicability. Hence the estimates presented in Sec. V (and in particular Tables III and IV) can serve only as first approximations, and to motivate considerably more accurate calculations and additional measurements.

Nevertheless, Secs. II–V and Tables III and IV suggest that the pinch specifications defined in the initial double-pinch-hohlraum design study [1], and the ICF-accelerator specifications presented in [43–45], may need to be modified.

These specifications implicitly assume that a $R=\ell = 10$ mm pinch with a 63-MA peak current and 100–120 ns implosion time would radiate a peak x-ray power of 1200 TW (2400 TW from two pinches) in a 7-ns pulse. As indicated by Tables III and IV, this assumption would be reasonable assuming idealized RT scaling. However, as demonstrated in Ref. [29], the scaling for pinches of interest to ICF is less favorable. For example, assuming Eqs. (16), (20), and (38), we estimate that at 63 MA and 120 ns, the peak x-ray power would be 380 TW per pinch, and the pulse width, 33 ns.

As indicated by Tables III and IV, when $R=\ell=10$ mm, decreasing τ_i from 100–120 ns to 56–63 ns would (for an ablatian-dominated pinch) produce x-ray parameters closer to those required to realize high-yield fusion.

However, reducing τ_i is only one approach to addressing the current-scaling problem uncovered in Ref. [29]. As discussed in Sec. III C 3 of Ref. [29], it is conceivable that an improved understanding of z-pinch physics would permit a more favorable scaling to be achieved. We note, for example, that the pinch models presented in Secs. II A and II B do not account for effects due to the polarity of the coaxial structure within which the pinch resides [94]. Seminal experiments by Sarkisov *et al.* [94] suggest that the performance of wire arrays could be improved by reversing the polarity that is presently used on the Z accelerator.

It is also possible that the hohlraum efficiency could be increased above the levels assumed here. Tables III and IV show a dramatic reduction in the requisite values of P_a and E_a when the anode-cathode gap of the pinch is decreased from 4 to 2 mm (when $R=\ell=10$ mm) and demonstrate that much can be gained by developing a more efficient system.

We speculate that achieving z-pinch-driven fusion will likely be predicated on progress in all of these areas: it will likely require advances in short-pulse high-current accelerator technology, an increase in the x-ray-power current-scaling exponent above the value of 1.24 ± 0.18 obtained in Ref. [29], and a more efficient z-pinch-driven hohlraum.

Such advances would probably require that the assumptions implicit in the estimates of Table III and IV be modified; however, the integrated and self-consistent approach

based on idealized scaling relations developed in Secs. II–V can be readily adapted to a different set of conditions.

ACKNOWLEDGMENTS

The authors would very much like to thank J. Bailey, G. Bennett, D. Bliss, J. Chittenden, J. De Groot, M. Douglas, R. Flora, S. Glaros, R. M. Green, D. Hammer, M. Horry, D. Jobe, M. Johnson, S. Lazier, S. Lebedev, L. Longmire, R. Olson, Y. Maron, J. Mills, L. P. Mix, T. Mulville, D. Peterson, J. Pyle, P. Reynolds, D. Romero, T. Romero, L. Ruggles, G. Sarkisov, J. J. Seamen, W. Simpson, S. Slutz, R. Smelser, J. Trammell, A. Velikovich, and M. Vigil for invaluable contributions, and D. Bliss, T. Cutler, and S. Slutz for graciously reviewing this article. We also wish to thank our colleagues at Sandia National Laboratories, Ktech Corporation, Team Specialty Products, Tri-Tech Machine Tool Company, Gull Group, Bechtel, C-Lec Plastics, Cornell University, EG&G, Imperial College, Lawrence Livermore National Laboratory, Los Alamos National Laboratories, Mission Research Corporation, Naval Research Laboratory, Prodyn Technologies, Titan-Pulse Sciences Division, the University of California, the University of Nevada, the University of New Mexico, Votaw Precision Technologies, and the Weizmann Institute for critical discussions. Sandia is a multiprogram laboratory operated by Sandia Corporation, a Lockheed Martin Company, for the United States Department of Energy's National Nuclear Security Administration under Contract DE-AC04-94AL85000.

APPENDIX: IGNITION MARGIN

We present here scaling relations for the ignition margin M and remaining fuel kinetic energy at ignition f_{ke} of an ICF capsule.

One can conceive of several reasonable definitions for the margin M; we adopt here the definition given in Ref. [86]. We consider an ICF capsule that has a 1D thermonuclear gain >1—i.e., a thermonuclear yield greater than E_c, the energy absorbed by the capsule during its implosion. We assume that the energy is delivered to the capsule by the hohlraum radiation incident upon the capsule, and that this radiation creates an ablation pressure that drives the implosion. For such a system we define M as

$$M \equiv \frac{E_f}{E_{f,ign}}, \tag{A1}$$

where E_f is the peak kinetic energy of the capsule's DT-fuel mass, and $E_{f,ign}$ is the minimum value of E_f that would be required for that capsule to achieve a thermonuclear gain of 1 (i.e., the minimum fuel kinetic energy required to achieve ignition).

We consider capsules with similar internal geometries, and drive pressures with similar time histories, so that to a reasonable approximation

$$E_f \propto m_f v_c^2 \propto P_f R_f^3 \propto \frac{P_f m_f \zeta}{\rho_0}. \tag{A2}$$

[Equation (A2) assumes $\zeta \gg 1$.] Combining Eqs. (64), (65), and (A2), and assuming ρ_0 is held constant, we obtain

$$v_c \propto \zeta^{1/2} P_f^{1/2} \propto \zeta^{1/2} P_c^{1/2} \propto \zeta^{1/2} T_r^{1.75}. \tag{A3}$$

Equation (A3) is consistent to within 4% with the parameters of the three National Ignition Facility capsule designs presented in Fig. 2–12 of Ref. [91]. (For these three designs, T_r ranges from 250 to 350 eV.)

The minimum fuel kinetic energy required to achieve ignition $E_{f,ign}$ scales as [86]

$$E_{f,ign} \propto m_f v_{ign}^2 \propto \frac{\alpha_{if,ign}^{1.88}}{v_{ign}^{5.89} P_{f,ign}^{0.77}}, \tag{A4}$$

where v_{ign}, $\alpha_{if,ign}$, and $P_{f,ign}$ are the peak fuel-implosion velocity, in-flight fuel adiabat, and peak fuel drive pressure of a minimally ignited capsule. Assuming $\alpha_{if,ign}=\alpha_{if}$, $P_{f,ign} \propto (v_{ign}^2/\zeta)$ [as suggested by Eq. (A3)], and $R_f \propto R_c$, we combine Eqs. (A1)–(A4) to obtain

$$M \propto \frac{R_c^{0.64} \zeta^{0.62} T_r^{3.5}}{\alpha_{if}^{0.40}}. \tag{A5}$$

In the literature, the margin is usually quoted as the remaining implosion kinetic energy of the fuel at ignition, as a fraction of the peak kinetic energy, and is determined by a 1D LASNEX capsule-implosion simulation [1,91]. Labeling this fraction as f_{ke}, we estimate that

$$f_{ke} \sim 1 - \frac{1}{M}. \tag{A6}$$

The $R_c=2.65$ mm capsule design assumed for Tables III and IV is the base line developed by Vesey *et al.* [11,12]. The parameters of this design are given in Fig. 5 and Table II. For this capsule, 1D LASNEX finds that $f_{ke}=26\%$; hence we infer that $M \sim 1.35$. The $R_c=4.82$ mm capsule assumed for Tables III and IV is a scaled version of the base-line design, with ζ, T_r, α_{if}, IFAR, v_c, and the fuel convergence ratio held constant at the values listed in Table II. Assuming Eqs. (A5) and (A6), and that $f_{ke}=26\%$ when $R_c=2.65$ mm, we estimate that $f_{ke}=49\%$ for the larger capsule, as indicated in Tables III and IV.

[1] J. H. Hammer, M. Tabak, S. C. Wilks, J. D. Lindl, *et al.*, Phys. Plasmas **6**, 2129 (1999).

[2] R. J. Leeper *et al.*, Nucl. Fusion **39**, 1283 (1999).

[3] M. E. Cuneo, R. A. Vesey, J. H. Hammer, J. L. Porter, Jr., *et al.*, Laser Part. Beams **19**, 481 (2001).

[4] M. E. Cuneo, R. A. Vesey, J. L. Porter, Jr., G. A. Chandler, *et al.*, Phys. Plasmas **8**, 2257 (2001).

[5] M. E. Cuneo, R. A. Vesey, J. L. Porter, Jr., G. R. Bennett, *et al.*, Phys. Rev. Lett. **88**, 215004 (2002).

[6] G. R. Bennett, M. E. Cuneo, R. A. Vesey, J. L. Porter, *et al.*,

Phys. Rev. Lett. **89**, 245002 (2002).
[7] D. L. Hanson, R. A. Vesey, M. E. Cuneo, J. L. Porter, Jr., *et al.*, Phys. Plasmas **9**, 2173 (2002).
[8] R. A. Vesey, M. E. Cuneo, G. R. Bennett, J. L. Porter, Jr., *et al.*, Phys. Rev. Lett. **90**, 035005 (2003).
[9] G. R. Bennett, R. A. Vesey, M. E. Cuneo, J. L. Porter, Jr., *et al.*, Phys. Plasmas **10**, 3717 (2003).
[10] R. A. Vesey, M. E. Cuneo, J. L. Porter, Jr., R. G. Adams, *et al.*, Phys. Plasmas **10**, 1854 (2003).
[11] R. A. Vesey, M. E. Cuneo, G. R. Bennett, D. L. Hanson, *et al.*, Bull. Am. Phys. Soc. **48**, 207 (2003).
[12] R. A. Vesey *et al.* (unpublished).
[13] C. L. Olson, in *Landholt-Boernstein Handbook on Energy Technologies*, Vol. VIII/3 of *Fusion Technologies*, edited by K. Heinloth (Springer-Verlag, Berlin-Heidelberg, 2005).
[14] R. E. Olson, Fusion Sci. Technol. **47**, 1147 (2005).
[15] M. D. Rosen, Phys. Plasmas **3**, 1803 (1996).
[16] J. E. Bailey, G. A. Chandler, D. Cohen, M. E. Cuneo, *et al.*, Phys. Plasmas **9**, 2186 (2002).
[17] J. M. Foster, B. H. Wilde, P. A. Rosen, T. S. Perry, *et al.*, Phys. Plasmas **9**, 2251 (2002).
[18] C. Deeney and R. B. Spielman (unpublished).
[19] J. L. Porter, Bull. Am. Phys. Soc. **42**, 1948 (1997).
[20] K. L. Baker, J. L. Porter, L. E. Ruggles, G. A. Chandler, *et al.*, Appl. Phys. Lett. **75**, 775 (1999).
[21] K. L. Baker, J. L. Porter, L. E. Ruggles, R. E. Chrien, and G. C. Idzorek, Rev. Sci. Instrum. **70**, 1624 (1999).
[22] K. L. Baker, J. L. Porter, L. E. Ruggles, D. L. Fehl, *et al.*, Rev. Sci. Instrum. **70**, 2012 (1999).
[23] K. L. Baker, J. L. Porter, L. E. Ruggles, G. A. Chandler, *et al.*, Phys. Plasmas **7**, 681 (2000).
[24] M. E. Cuneo, G. A. Chandler, R. A. Vesey, J. L. Porter, *et al.*, Bull. Am. Phys. Soc. **46**, 234 (2001).
[25] M. Mazarakis, M. Douglas, M. Cuneo, G. Chandler, T. Nash, and W. Stygar, Bull. Am. Phys. Soc. **46**, 27 (2001).
[26] W. A. Stygar, R. E. Olson, R. B. Spielman, and R. J. Leeper, Phys. Rev. E **64**, 026410 (2001).
[27] M. G. Mazarakis *et al.*, *Proceedings of the 29th IEEE International Conference on Plasma Science* (IEEE, Piscataway, NJ , 2002), p. 105.
[28] M. Mazarakis, C. Deeney, W. Stygar, T. Nash, *et al.*, Bull. Am. Phys. Soc. **47**, 189 (2002).
[29] W. A. Stygar, H. C. Ives, D. L. Fehl, M. E. Cuneo, *et al.*, Phys. Rev. E **69**, 046403 (2004).
[30] E. M. Waisman, M. E. Cuneo, W. A. Stygar, R. W. Lemke, *et al.*, Phys. Plasmas **11**, 2009 (2004).
[31] D. B. Sinars, M. E. Cuneo, E. P. Yu, D. E. Bliss, *et al.*, Phys. Rev. Lett. **93**, 145002 (2004).
[32] M. E. Cuneo *et al.*, Phys. Rev. E **71**, 046406 (2005).
[33] M. G. Mazarakis *et al.*, manuscript in preparation (2005).
[34] R. B. Spielman *et al.*, in *Proceedings of the 11th IEEE International Pulsed Power Conference*, edited by G. Cooperstein and I. Vitkovitsky (IEEE, Piscataway, NJ, 1997), p. 709.
[35] P. A. Corcoran *et al.*, in *Proceedings of the 11th IEEE International Pulsed Power Conference [34]*, p. 466.
[36] R. J. Garcia *et al.*, in *Proceedings of the 11th IEEE International Pulsed Power Conference [34]*, p. 1614.
[37] H. C. Ives *et al.*, in *Proceedings of the 11th IEEE International Pulsed Power Conference [34]*, p. 1602.
[38] M. A. Mostrom *et al.*, in *Proceedings of the 11th IEEE International Pulsed Power Conference [34]*, p. 460.
[39] R. W. Shoup *et al.*, in *Proceedings of the 11th IEEE International Pulsed Power Conference [34]*, p. 1608.
[40] I. D. Smith *et al.*, in *Proceedings of the 11th IEEE International Pulsed Power Conference [34]*, p. 168.
[41] K. W. Struve *et al.*, in *Proceedings of the 11th IEEE International Pulsed Power Conference [34]*, p. 162.
[42] W. A. Stygar *et al.*, in *Proceedings of the 11th IEEE International Pulsed Power Conference [34]*, p. 591.
[43] K. W. Struve and D. H. McDaniel, in *Proceedings of the 12th International Conference on High-Power Particle Beams (Beams '98)*, edited by M. Markovits and J. Shiloh (IEEE, Haifa, Isreal, 1998), p. 334.
[44] K. W. Struve *et al.*, in *Proceedings of the 12th IEEE International Pulsed Power Conference*, edited by C. Stallings and H. Kirbie (IEEE, Piscataway, NJ, 1999), p. 493.
[45] D. H. McDaniel *et al.*, in *Fifth International Conference on Dense Z Pinches*, edited by J. Davis, C. Deeney, and N. Pereira, AIP Conf. Proc. No. 651 (AIP, Melville, NY, 2002), p. 23.
[46] E. J. Yadlowsky, J. J. Moschella, R. C. Hazelton, T. B. Settersten, *et al.*, Phys. Plasmas **3**, 1745 (1996).
[47] J. P. Chittenden, S. V. Lebedev, A. R. Bell, R. Aliaga-Rossel, *et al.*, Phys. Rev. Lett. **83**, 100 (1999).
[48] J. P. Chittenden, S. V. Lebedev, J. Ruiz-Camacho, F. N. Beg, *et al.*, Phys. Rev. E **61**, 4370 (2000).
[49] S. V. Lebedev, F. N. Beg, S. N. Bland, J. P. Chittenden, *et al.*, Phys. Rev. Lett. **85**, 98 (2000).
[50] V. V. Aleksandrov, A. V. Branitskii, G. S. Volkov, E. V. Grabovskii, *et al.*, Fiz. Plazmy **27**, 99 (2001) [Plasma Phys. Rep. **27**, 89 (2001)].
[51] J. P. Chittenden, S. V. Lebedev, S. N. Bland, F. N. Beg, and M. G. Haines, Phys. Plasmas **8**, 2305 (2001).
[52] S. V. Lebedev, F. N. Beg, S. N. Bland, J. P. Chittenden, *et al.*, Phys. Plasmas **8**, 3734 (2001).
[53] D. B. Reisman, J. H. Hammer, A. Toor, and J. S. De Groot, Laser Part. Beams **19**, 403 (2001).
[54] V. V. Alexandrov, I. N. Frolov, M. V. Fedulov, E. V. Grabovsky, *et al.*, IEEE Trans. Plasma Sci. **PS-30**, 559 (2002).
[55] J. P. Chittenden, S. V. Lebedev, B. V. Oliver, E. P. Yu, and M. E. Cuneo, Phys. Plasmas **11**, 1118 (2004).
[56] S. V. Lebedev, D. J. Ampleford, S. N. Bland, S. Bott, *et al.*, in *Proceedings of the Third International Conference on Inertial Fusion Sciences and Applications, Monterey, CA, 2003*, edited by B. A. Hammel, D. D. Meyerhofer, J. Meyer-ter-Vehn, and H. Azechi (American Nuclear Society, La Grange Park, IL, 2004), p. 730.
[57] D. D. Ryutov, M. S. Derzon, and M. K. Matzen, Rev. Mod. Phys. **72**, 167 (2000).
[58] D. L. Peterson, R. L. Bowers, K. D. McLenithan, C. Deeney, *et al.*, Phys. Plasmas **5**, 3302 (1998).
[59] W. J. Duncan, *Physical Similarity and Dimensional Analysis* (Edward Arnold & Co., London, 1953).
[60] N. A. Bobrova, T. L. Razinkova, and P. V. Sasorov, Fiz. Plazmy **18**, 517 (1992) [Sov. J. Plasma Phys. **18**, 269 (1992)].
[61] I. R. Lindemuth, G. H. McCall, and R. A. Nebel, Phys. Rev. Lett. **62**, 264 (1989).
[62] C. A. Coverdale, C. Deeney, M. R. Douglas, J. P. Apruzese, *et al.*, Phys. Rev. Lett. **88**, 065001 (2002).
[63] T. W. L. Sanford, G. O. Allshouse, B. M. Marder, T. J. Nash, *et*

al., Phys. Rev. Lett. **77**, 5063 (1996).
[64] C. Deeney, T. J. Nash, R. B. Spielman, J. F. Seamen, *et al.*, Phys. Rev. E **56**, 5945 (1997).
[65] S. A. Pikuz, T. A. Shelkovenko, A. R. Mingaleev, D. A. Hammer, and H. P. Neves, Phys. Plasmas **6**, 4272 (1999).
[66] M. P. Desjarlais (unpublished).
[67] D. L. Peterson, R. L. Bowers, J. H. Brownell, A. E. Greene, *et al.*, Phys. Plasmas **3**, 368 (1996).
[68] J. A. Hammer, J. L. Eddleman, P. T. Springer, M. Tabak, *et al.*, Phys. Plasmas **3**, 2063 (1996).
[69] M. R. Douglas, C. Deeney, and N. F. Roderick, Phys. Plasmas **5**, 4183 (1998).
[70] B. M. Marder, T. W. L. Sanford, and G. O. Allshouse, Phys. Plasmas **5**, 2997 (1998).
[71] D. L. Youngs, Physica D **12**, 32 (1984).
[72] D. L. Youngs, Phys. Fluids A **3**, 1312 (1991).
[73] M. P. Desjarlais and B. M. Marder, Phys. Plasmas **6**, 2057 (1999).
[74] M. R. Douglas, C. Deeney, R. B. Spielman, C. A. Coverdale, *et al.*, Phys. Plasmas **7**, 1935 (2000).
[75] R. B. Spielman, C. Deeney, G. A. Chandler, M. R. Douglas, *et al.*, Phys. Plasmas **5**, 2105 (1998).
[76] C. Deeney, D. L. Peterson, R. B. Spielman, K. W. Struve, and G. A. Chandler, Phys. Plasmas **5**, 2605 (1998).
[77] M. R. Douglas, C. Deeney, R. B. Spielman, C. A. Coverdale, *et al.*, Phys. Plasmas **7**, 1935 (2000).
[78] W. A. Stygar, G. A. Chandler, D. L. Fehl, T. L. Gilliland, *et al.* (unpublished).
[79] T. W. L. Sanford, R. B. Spielman, G. O. Allshouse, G. A. Chandler, *et al.*, IEEE Trans. Plasma Sci. **PS-26**, 1086 (1998).
[80] J. R. Taylor, *An Introduction to Error Analysis* (University Science, Sausalito, CA, 1997).
[81] W. A. Stygar *et al.*, Phys. Rev. ST Accel. Beams **7**, 070401 (2004).
[82] A. Ron, A. A. Mondelli, and N. Rostoker, IEEE Trans. Plasma Sci. **PS-1**, 85 (1973).
[83] J. M. Creedon, J. Appl. Phys. **48**, 1070 (1977).
[84] C. W. Mendel, Jr., D. B. Seidel, and S. E. Rosenthal, Laser Part. Beams **1**, 311 (1983).
[85] M. M. Basko and J. Johner, Nucl. Fusion **38**, 1779 (1998).
[86] M. C. Herrmann, M. Tabak, and J. D. Lindl, Phys. Plasmas **8**, 2296 (2001).
[87] J. D. Lindl, *Inertial Confinement Fusion* (Springer-Verlag, New York, 1998).
[88] R. A. Vesey and T. A. Mehlhorn, Bull. Am. Phys. Soc. **43**, 1903 (1998).
[89] R. A. Vesey, M. Cuneo, D. Hanson, J. Porter, *et al.*, Bull. Am. Phys. Soc. **44**, 227 (1999).
[90] M. D. Rosen (unpublished).
[91] J. D. Lindl, P. Amendt, R. L. Berger, S. G. Glendinning, *et al.*, Phys. Plasmas **11**, 339 (2004).
[92] T. W. L. Sanford, R. C. Mock, T. J. Nash, K. G. Whitney, *et al.*, Phys. Plasmas **6**, 1270 (1999).
[93] W. A. Stygar *et al.*, in *Proceedings of the 11th IEEE International Pulsed Power Conference [34]*, p. 1258.
[94] G. S. Sarkisov, P. V. Sasorov, K. W. Struve, D. H. McDaniel, *et al.*, Phys. Rev. E **66**, 046413 (2002).